Large-Scale Motor Dynamics Associated with Reaching are Altered in Essential Tremor

Timothy O. West[1,2], Kenan Steidel[3], Tjalda Flessner[3], Alexander Calvano[3], Deniz Kucukahmetler[1], Marielle J. Stam[4], Meaghan E. Spedden[2], Benedikt Wahl[5], Veikko Jousmäki[6], John Eraifej[7], Ashwini Oswal[7], Tabish A. Saifee[8], Gareth Barnes[2], Simon F. Farmer[8,9], David J. Pedrosa[3,10], Hayriye Cagnan[1,2]

[1] *Department of Bioengineering, Sir Michael Uren Hub, Imperial College London, London, W12 0BZ, UK*

[2] *Wellcome Trust Centre for Human Neuroimaging, UCL Queen Square Institute of Neurology, University College London, London, WC1N 3AR, UK*

[3] *Department of Neurology, Philipps-University Marburg, 35041 Marburg, Germany*

[4] *Department of Neurology, Amsterdam University Medical Centers, Amsterdam Neuroscience, University of Amsterdam, Amsterdam, the Netherlands*

[5] *Faculty of Electrical Engineering and Information Technology, RWTH Aachen University, 52062 Aachen, Germany*

[6] *Aalto Neuroimaging, Aalto University, Espoo, Finland*

[7] *Medical Research Council Brain Network Dynamics Unit, Nuffield Department of Clinical Neurosciences, University of Oxford, Mansfield Road, Oxford OX1 3TH, UK.*

[8] *Department of Neurology, National Hospital for Neurology & Neurosurgery, Queen Square, London WC1N 3BG, UK.*

[9] *Department of Clinical and Movement Neurosciences, UCL Institute of Neurology, Queen Square, London WC1N 3BG, UK*

[10] *Centre of Mind, Brain and Behaviour, Philipps-University Marburg, 35041 Marburg, Germany*

Abstract

Introduction: Essential Tremor (ET) is a common neurological disorder identified by involuntary rhythmic movements stemming from pathological synchronization within a network that overlaps significantly with the normal motor circuit. The efficacy of therapeutic brain stimulation for ET is impeded by a limited understanding of how tremor-related synchronization affects brain circuits and disrupts normal sensorimotor processing. This paper details the changes in brain-wide synchronization associated with ET and connects these to the oscillatory dynamics during voluntary movements. **Methods:** We used high-density electroencephalography (EEG, 11 controls, 12 patients), and for the first time in ET patients, optically pumped magnetoencephalography (OPM, 5 controls, 4 patients) to record brain activity during upper limb reaching. We localized and analysed brain sources that synchronize with pathological tremors, studying motor oscillations in these regions. Using a novel dimensionality reduction approach, we identified a set of simple, latent circuits with specific frequency characteristics and analysed their relationship to kinematics and tremor. **Results:** Despite slight reductions in velocity, ET patients demonstrated reaching movements with kinematics comparable to controls. Notably, key motor areas - including the supplementary motor area, lateral

prefrontal cortex, posterior parietal cortex, and motor cerebellum - were synchronized to tremor frequencies. Motor oscillations were significantly changed in patients with ET relative to controls, including a 15% increase in movement responsive desynchronization in the low beta (14-21 Hz) band which inversely correlated with tremor severity. Oscillations in the beta and theta bands were key predictors of patients` overall tremor levels. Latent state analysis in EEG and OPM data located these changes to fronto-parietal and premotor/prefrontal circuits. High tremor trials were associated with diminished post-movement beta rebound in frontoparietal and premotor circuits and an increase in sensorimotor gamma activity (30-60 Hz). Latent dynamics were predictive of changes in patients` movement velocity and hold stability, suggesting that increased movement related beta desynchronization may reflect a compensatory mechanism in the brain. **Conclusions:** This study demonstrates that ET leads to significant changes in the oscillatory dynamics within individual motor regions and broader networks. Specifically, we suggest that increased desynchronization of networks in ET enables successful execution of movement, by freeing neural resources otherwise entrained by pathological synchronization at tremor frequencies. Our findings, reproducible across both EEG and OPM recordings, underline how motor-related brain signals can predict subject level tremor severity and offer a new set of candidate biomarkers crucial for developing advanced closed-loop stimulation therapies for ET.

1 Introduction

Essential Tremor (ET) is a common neurological disorder characterized by involuntary rhythmic movements affecting the limbs, head, or trunk[1]. Over 50% of ET patients are unresponsive to pharmacological interventions[2]. Surgical lesioning of the thalamus can be effective, yet it is by necessity unilateral, irreversible, and in many cases, tremor may re-emerge[3]. For the most severely affected patients, deep brain stimulation (DBS) of the ventrolateral thalamus provides an adaptable and bilateral therapy. However, patients require permanent device insertion and over time, 70% of patients receiving continuous DBS lose benefit[4,5]. In some cases, this can be alleviated with regular reparameterization of the stimulator, but this is complex, time-consuming, and not always successful[6].

These challenges motivate the development of next generation neurostimulation for ET that aims to: (a) be minimally invasive compared to lesioning and (b) capable of providing closed-loop, on-demand stimulation matched to tremor episodes' severity. Non-invasive stimulation can provide an alternative to DBS but requires targets that are accessible without surgery. For instance, peripheral nerve stimulation[7–10] has been trialled with mixed success. These studies follow the rationale that tremor is modulated by afferent input to the thalamus[11]. Tonic peripheral stimulation may act as a reversible afferent block, or when delivered phase locked to tremor acceleration, can provide tremor suppression via phase cancellation of a central tremor oscillator[12]. Existing closed loop approaches for stimulation

in ET have explored using inertial and/or myographic tremor signals[13–16] but are limited to providing reactive control and are subject to variabilities associated with changes in motor task, inertial loading, and posture. Moreover, the use of peripheral signals to suppress tremors via closed-loop stimulation is complicated by the inconsistent connection between central tremor origins and muscle activity[17,18]. A more effective strategy might involve directly targeting the central tremor sources in the brain.

A wealth of neuroimaging work supports the existence of a distributed tremor circuit in the brain[19,20], involving the thalamus, cerebellum, parietal, and motor cortex. This network has been established through both hemodynamic correlates of tremor[21–24] and also electrophysiological signals measured using electroencephalography (EEG)[25–27] and magnetoencephalography (MEG) [28]. Electrophysiological signals are particularly promising for closed-loop stimulation, as they rapidly respond to—and can even predict—tremor fluctuations. To date, non-invasive brain stimulation has targeted the primary motor cortex[29,30] or the cerebellum[15,31–33], with the latter demonstrating superior clinical outcomes. Despite this, most approaches to stimulation remain open-loop and require high stimulation energies that can be uncomfortable for the patient.

Instead of direct stimulation, components of the identified tremor circuit could enhance control of stimulation in therapies such as DBS to the ventrolateral thalamus. Similar abnormal neural oscillations play a role in other movement disorders (e.g., Parkinson's and Dystonia) where therapeutic stimulation aims to normalize large-scale brain network dynamics[34,35]. The significant overlap of the tremor circuit with volitional motor control networks[36,37] implies that common signals, such as 14-30 Hz beta band oscillations, could predict tremor onsets. For example, movement responsive beta band event related desynchronization (ERD)[38] has been used to trigger DBS in tremor[39–41] at the onset of action or postural tremors, offering a method for anticipatory control. However, it remains unclear how this aberrant synchronization at tremor frequencies affects the physiological markers of motor processing. Most EEG studies have adopted a static approach, focusing on tremor during unchanging postures, and thus ignored the dynamic changes in motor control associated with ET, especially during active limb movements like reaching[42–44].

We hypothesised that the pathophysiology of ET disrupts the large-scale motor dynamics associated with naturalistic movement, such as reaching. To investigate this, we utilize advances in whole-brain neuroimaging to examine how circuits in the brain are comodulated by both pathological tremor and the generation of voluntary movements. Utilizing high-density EEG and introducing optically pumped MEG (OPM)[45] to ET studies for the first time, we localized oscillatory brain activity that both synchronizes with tremors and reacts to movement. The advent of OPM has helped facilitate high resolution brain recordings during naturalistic human movement[46,47] and enhanced detection of high-frequency brain rhythms[48].

To aid interpretation of high-resolution neuroimaging recorded across multiple regions and frequencies we use time frequency principal component analysis (tfPCA)[49]. This dimensionality reduction method allows us to decompose time locked, movement responsive oscillations recorded over the brain, into simplified components with associated *latent* dynamics. These low dimensional dynamics summarise how the brain acts in concert during movement and tremor, tying regions and frequency bands into ensemble circuits with correlated activities—akin to sections of an orchestra. We evaluate whether these latent representations of whole brain recordings may provide candidate signals for closed control. Latent space analyses have proven effective at prediction of behaviour from brain signals at the single trial level[50,51] but deployment in whole-brain human neuroimaging is in its nascency[52–54].

Using these tools, we localized large regions of the cortex and cerebellum that are synchronized to pathological ET. In these same regions, we then examined classic movement responsive oscillations for changes associated with ET pathophysiology. With the aim of establishing novel biomarkers for future stimulation approaches in mind, we asked whether these same signals were predictive of tremor severity at either the trial or subject level, and to what extent changes reflect adaptive dynamics to compensate for pathological synchronization in ET.

Methods

2.1 Recruitment and Details of Participants

Ethical approvals were obtained from the respective committees of the Philipps-University Marburg, University College London, and University College London Hospital. Consent was obtained according to the Declaration of Helsinki. UK clinical ethics were approved by the Health Research Authority (REC 20/WA/0124). EEG experiments were conducted with 16 patients (44 ±20 years of age, 6 female) diagnosed with essential tremor (ET) and 15 controls (45 ±20 years of age, 6 female). Diagnosis was made by a movement disorder specialist according to the clinical MDS-criteria[55]. OPM was conducted with 4 ET patients (50 ±20 years of age, 1 female) and 5 healthy controls (50 ±13 years of age, 1 female). All patients displayed a mild to moderate upper limb tremor, scoring between 3 and 6 on unilateral “The Essential Tremor Rating Assessment Scale” (TETRAS, Elble, 2016). The EEG cohort (Marburg) had a mean TETRAS performance score of 17.0 ±2.5 and the OPM cohort (London) had scores of 19.5 ±3.8. A minority of the EEG cohort displayed mild head tremor (4/12 patients scoring 1, 1/12 scoring 2). Clinical details and relevant medication for the patients are given in tables in appendix I and II.

2.2 Delayed Reach-to-Target Task

To probe the interaction between tremor and voluntary motor control, participants performed a delayed reach to target task, making whole limb reaches to mimic naturalistic movement. The task (Figure 1A) required participants to adopt a 90-degree upper arm elevation against gravity with flexed elbow posture and then, from this position, make centre-out reaches and then hold their finger fixed to "pop" target balloons. The task sequence was: (a) 3 s eyes-open rest, (b) 3 s postural (as above) hold, (c) 2.5 ±1 s presentation of movement cues, given as arrows of varying length, (d) appearance of a GO cue to initiate a reach, to one of eight targets, (e) 1.5 s of sustained hold required to "pop" the balloon. A point was scored if the correct balloon was popped (as predicted from the dispersion of the arrows). A maximum of 4 s was given to make the reach and hold. In addition, 30 s of rest and postural hold (i.e., the posture described above) was recorded for each block. We recorded 6 sessions of 24 reaches (~12 minutes each), yielding an average of 144 reaches per participant.

The task followed a 2x2 design manipulating cue uncertainty and target size. Cue uncertainty was set to be low or high (LUC and HUC, respectively), by changing the dispersion of arrows (see appendix III for details) titrated to success rates of 85% and 15%, respectively. The size of the targets (i.e., the balloons) were either small or large (SML and LRG, respectively). For EEG recordings the task was presented on an LCD monitor (30 x 53 cm, 60 Hz, SML/LRG diameters: 1.4/3.6 cm) placed at arm's length from the participant. For OPM recordings, the task was presented via a projector to a screen (42 x 70 cm, 60 Hz, SML/LRG diameters: 2/5 cm).

2.3 High Density Electroencephalography

High-density EEG (HD-EEG) was recorded in a recording chamber using an elastic cap to mount active, gel-based electrodes (Brain Products GmBH, Gilching, Germany) in the standard 10-10 system with 128 electrodes and amplified using a Brain Products DC amp. Electrode gel was applied to maintain electrode impedance below 10 kΩ. All data were recorded with a 1 kHz low pass filter and digitized at 5 kHz. EEG recordings were made with a reference at FCz, which was re-referenced offline to the common average.

2.4 Optically Pumped Magnetometer Recordings

Optically pumped magnetoencephalography (OPM) was made using a combination of 2nd and 3rd generation QuSpin sensors (dual- and tri-axial sensors, respectively; QuSpin Inc., Louisville, Colorado, USA) mounted in rigid 3D-printed casts (Chalk Studios, London, UK) custom-built to each participant's scalp shape determined from structural magnetic resonance images (MRIs). In the absence of an MRI (1 control and 1 patient), the head shape was estimated using an infrared depth camera. Offsets of 1-3 mm were added to scanner casts to allow for anatomical error, tissue deformation, and hair.

OPM experiments were conducted in a magnetically shielded room (MSR; Magnetic Shields Ltd, Staplehurst, UK). The inner layer of mu-metal lining the room was degaussed using a low-frequency decaying sinusoid driven through cables within the walls before the start of the experiment. The OPM sensors were then nulled using onboard nulling coils and calibrated. The OPM acquisition system (National Instruments, Texas, USA) had a sampling frequency of 6 KHz and a 16-bit resolution. An antialiasing 500 Hz low-pass filter (60th order FIR filter combined with a Kaiser window) was applied before data were down-sampled offline to 2 kHz.

2.5 Kinematics and Accelerometery Recordings

Arm movement was captured with Optitrack Motive software (Planar Systems, Oregon, USA) and an infrared camera (Optitrack Duo/Trio) tracking a reflective marker attached to the participant's hand. Task triggers were sent to the EEG amplifier using a LabJack U3 DAC (LabJack Corp., Colorado, USA). Acceleration was recorded via a triaxial sensor (EEG, Brainproducts GmBH; OPM; ADXL335; Analog devices Inc., Wilmington, Massachusetts, USA) affixed to the affected limb. For one EEG patient, accelerometery was not available, this participant is excluded from analyses requiring estimates of tremor (EEG/Acc. coherence and trial-by-trial tremor analyses). Statistics of movement kinematics were computed by averaging trials over each condition, removing outliers with |Z-score| > 1.96, and then computing an ANOVA.

2.6 Time Locking of Movement Data

The onsets of each postural raise were found from thresholding the Z-normalized sum of the triaxial accelerometers at Z = 3. Due to the large variability in reach movements, a semi-supervised method was used. Three independent scorers manually marked the execution and hold times, provided a quality score of 1-3 for movement traces (accelerometery and motion tracking) for each trial in a random subset of the data (30%). For precise criteria, please see appendix IV. These manual labels were then used to train a convolutional neural network (CNN) that we deployed on the full dataset. The CNN performance and cross-validation procedures are given in Supplementary Information I.

2.7 Preprocessing, Artefact Removal, and Data Rejection

Data were analysed using custom scripts written in MATLAB (The Mathworks, Massachusetts, USA) using the Fieldtrip[57] and SPM 12 toolboxes. Data were digitized and down sampled to 512 Hz. For EEG, individual channels were visually inspected to remove those affected by gross movement artefact, and then high and low pass filtered at 2 and 98 Hz using FIR windowed-sync filters. Line noise was removed by fitting sine and cosine components to the line frequency and then subtracting from the data. Eye blink, muscle, or cable artefacts were removed using independent component analysis (ICA). Trials with remaining artefacts were rejected visually, using Z-score and kurtosis measures. Finally, bad channels were replaced via local spline interpolation. OPM signals were

processed identically but used adaptive multipole model[58] for interference reduction following ICA. No channel interpolation was performed for missing or removed OPM channels.

We removed whole participants in the cases where the task sequence was not well followed (e.g., reaching directly from rest), greater than 75% of reaches being rejected by the CNN, or EEG data quality was poor (high prevalence of cable, movement or muscle artefact in the sensors). Finally, correlation measures were checked for outliers, using three times the mean Cook's distance as a threshold[59].

2.8 Source Space Analysis

Dynamic Imaging of Coherent Sources[60] (DICS) was used to map the distribution of power or coherence across the cortical volume. Wideband (2-98 Hz) beamformer weights were used to project sensor-level data to source-level virtual electrodes. We term coherence between inertial and M/EEG signals corticokinematic coherence, following Bourguignon et al., (2011). To maximise sensitivity of DICS to weakly synchronized sources, an auxiliary analysis used trials from the top 50% of coherence for contralateral supplementary motor area (cSMA; the peak of the group averaged image), and then regressed out the cSMA virtual channel signal, following Muthuraman et al., (2018). Brain parcellations used the Automated Anatomical Labelling atlas 3 [62]. For full details concerning the construction of forward models and sensor coregistration, please see appendix V.

Statistics in the source space were computed using either one-sample (DICS coherence in tremor band), or two-sample (ET/Control contrasts, cue locked contrasts) t-statistics. DICS images were first normalized to account for unequal sample size[11,63]. Statistical maps are presented as (a) t-statistics thresholded at the critical level ($P < 0.05$, uncorrected); and (b) overlap maps of the top 90th percentile of each subject.

2.9 Estimation of Tremor Magnitude

Tremor signals were estimated from the triaxial accelerometery (Supplementary Figure 2). Digitized voltage traces were converted to units of acceleration (m/s^2) using the conversion factors supplied by the manufacturer. We isolated the epochs of the task where tremor was expected – i.e., during the postural hold, post-cue onset, and following termination of the reach. For each epoch, we computed the principal component of the filtered triaxial accelerometer signal (4-12 Hz; bandpass FIR filter)[1]. The peak tremor frequency was then computed from the multitapered power spectrum (1.5 tapers/Hz) of the first component. Tremor amplitude was estimated by taking the root mean square of the signal filtered for a second time at the tremor peak ±3 Hz.

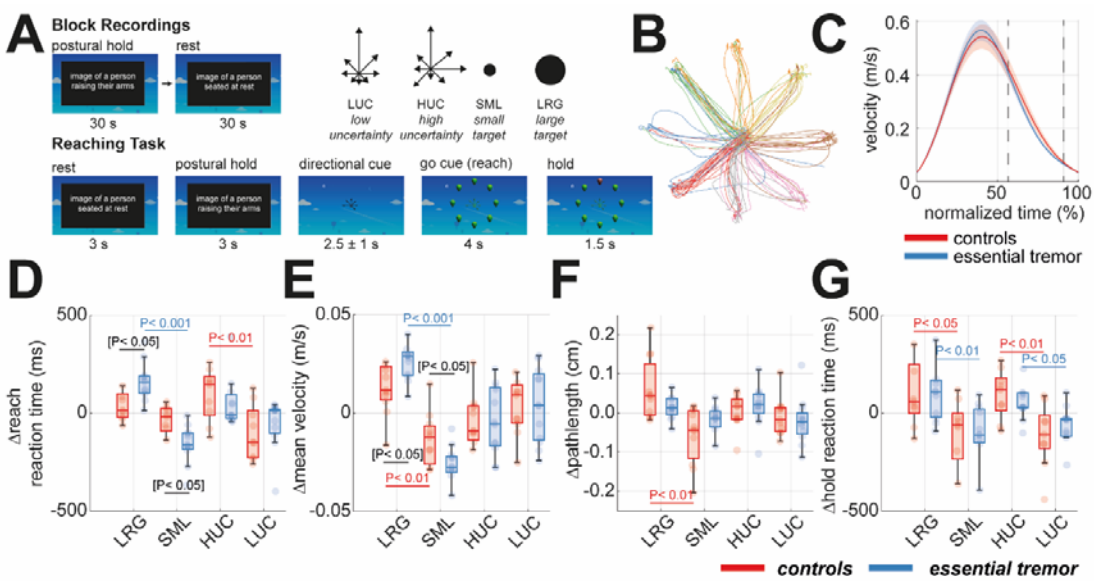

Figure 1–Structure of Delayed Reach-to-Target Task and Behavioural Analysis. (A) Illustration of the sequence and timings of the reaching task. Each block began with 30 s of postural hold and eyes open rest. The reaching task consisted of *rest* (3 s), *posture* (3 s), onset of directional *cue* (2.5 ±1 s), reach *execution* (max. 4 s), and sustained *hold* (1.5 s). The task followed a 2x2 design: high versus low uncertainty (HUC vs LUC), and large versus small targets (LRG vs SML). **(B)** An example set of trajectories from a single subject for the centre-out reaches, colour coded by the target. **(C)** The group averaged velocity profiles of the reaches, plot in normalized time from reach onset (0%) to hold onset (100%). **(D-E)** Boxplots summarising the between-subject statistics of task kinematics. Each point gives the deviation from the subject's mean value. Data is shown for EEG experiment controls (red) and ET patients (blue), with colour matched bars indicating significant post-hoc t-tests. Black bars indicate significant t-test when comparing ET and controls.

2.10 Tremor Prediction with Convolutional Neural Networks

We used a Convolutional Neural Network (CNN) to predict tremor severity from M/EEG time frequency images. Images were smoothed with a Gaussian kernel (full width half maximum: 1.17 Hz x 0.24 s). The CNN comprised of two layers, each including batch normalization, rectified linear unit activation functions, and dropout to prevent overfitting. We used an 80:20 training to testing split. Accuracy is reported as R^2, estimating the variance explained by the predicted features of the test data. The average accuracy of five independently trained replicates of the network are reported. Feature importance was computed using the Gradient-weighted Class Activation Mapping (Grad-CAM) algorithm.

Tremor prediction was performed in two ways – (1) between-subjects prediction of averaged severity; and (2) within-subjects prediction of trial-by-trial variation in tremor. At the group level, the tremor was left unnormalized, such that total variance in the between subject's tremor severity remained. At the single subject level, tremor was Z-score normalized, such that each subject's average tremor amplitude was removed.

2.11 Identifying Latent Spectro-Spatial Components with Time-Frequency Principal Component Analysis

We identified large-scale brain circuits associated with voluntary movement control and tremor using time-frequency Principal Components Analysis (tfPCA)[49]. tfPCA projects high dimensional time frequency data computed at voxels across the brain (time x frequency x space x repetitions) to a low dimensional "latent" description of dynamics (component x time). Voxels included regions of interest (ROIs) in the ipsi- and contra- lateral dorsal prefrontal cortex, primary and supplementary motor areas, posterior parietal cortex, and cerebellum lobule VI. All ROIs were identified from the DICS source localizations detailed in the results. tfPCA was applied to the group level data and then weights used to back-project data to the single trial level. For details of the implementation of tfPCA, and the back-projection, please see Appendix VI. To test changes associated with kinematics or tremor, we applied cluster-based permutation testing to data split by the 1st and 4th quartile of each subject, using P = 0.1 as a cluster forming threshold. Latent dynamics are compared across subjects or modalities using Pearson's R, as a measure of correlation.

3 Results

3.1 Behavioural Analyses of the Delayed Reach-to-Target Task

All participants performed the reaching task outlined in Figure 1A. 4/31 EEG participants were excluded as they did not follow the task sequence, and 4 additional EEG participants were removed due to large muscle/movement artefact (as determined by criteria outlined in methods). This left a total of 23 subjects for analysis (11 healthy controls, 12 ET patients). Nine participants were recorded with OPMs (5 controls, 4 ET patients) with none excluded.

Task performance and kinematics were similar between ET and control subjects and exhibited similar reaction times and pathlengths. ET patients reached with a slower average velocity (ANOVA (84), F-statistic = 4.76, $P < 0.05$) attributable to faster deceleration at the end of the reach (Figure 1C, region bordered by dashed line). Task related modulations were clearest after subtracting subject averages to eliminate between-subject variance. As expected, small target sizes resulted in slower reaction times in both the control and ET cohorts (Figure 1D; ANOVA (82), F-statistic = 37.7, $P < 0.001$). Both high cue uncertainty and small targets were accompanied by slower reach velocities (Figure 1E; Uncertainty: ANOVA (84), F-statistic = 14.1 $P < 0.001$; Size: ANOVA (84), F-statistic = 7.39, $P < 0.01$). Only control subjects showed changes in reach path length in response to target size (Figure 1F; t-test (20), t-statistic = 3.66, $P < 0.01$), suggesting

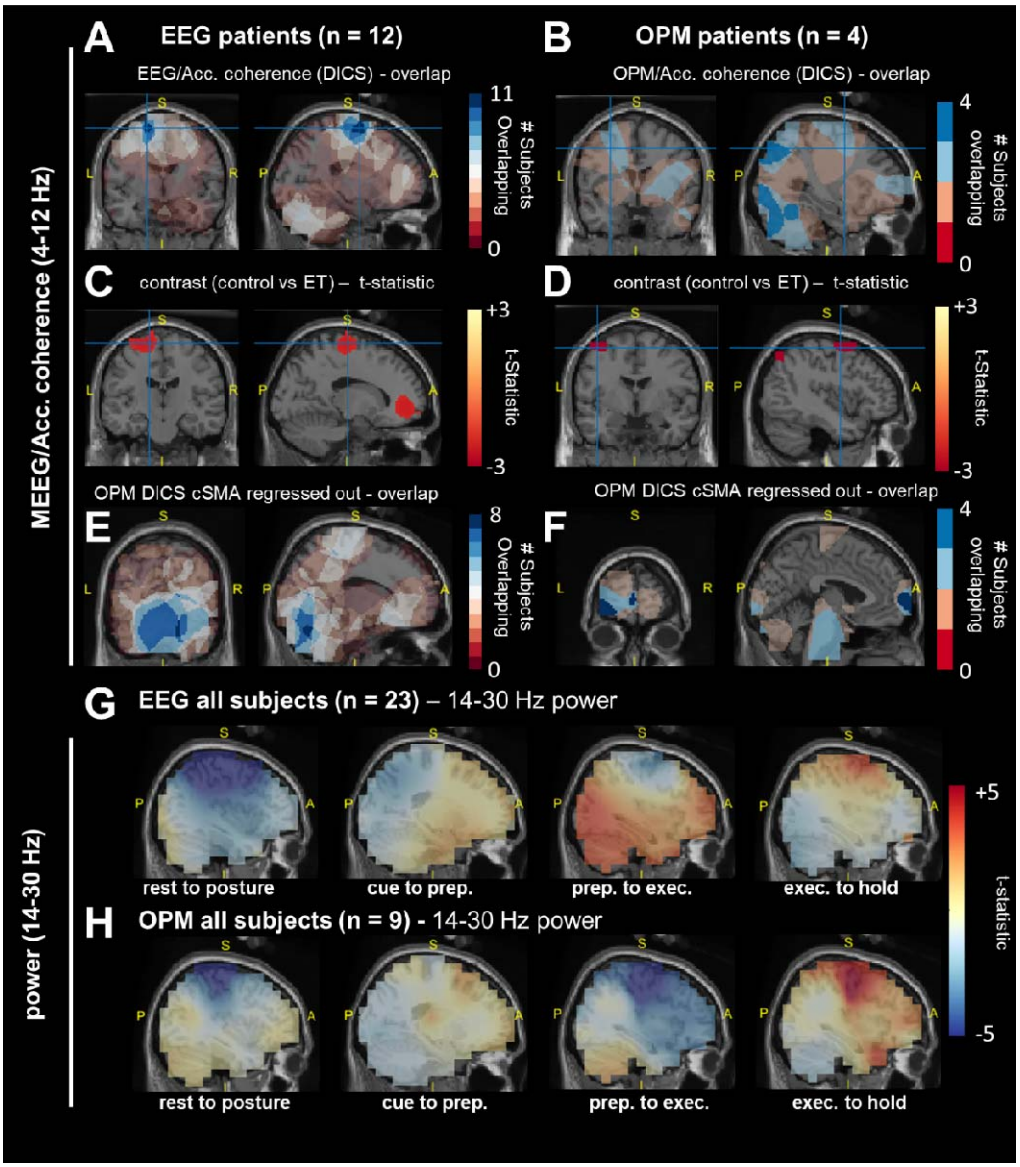

Figure 2 – Source maps of OPM/EEG data coherence with the 4-12 Hz peripheral tremor signal (A-F) estimated using a dynamic imaging of coherent sources (DICS) beamformer from postural hold data and movement related beta (14-30 Hz) power changes (G-H). Subjects' anatomy was flipped such that all slices were contralateral to the dominant hand prior to performing statistics. **(A and B)** EEG and OPM image of the overlap of the top 90th percentiles subject level coherence at source level. The slice location corresponds to the peak of the ET group average peak at the contralateral supplementary motor area (cSMA). **(C and D)** T-contrast of EEG and OPM DICS images comparing coherence in tremor band between Control and ET. Maps were thresholded at the critical T-value ($P < 0.05$, uncorrected). Positive T-statistics indicate Control > ET. **(E and F)** Same as (C and D) but for overlaps computed from the auxiliary DICS analysis, performed after regressing out the cSMA virtual channel. **(G and H)** Grand averaged EEG and OPM source power images across both controls and ET patients. Contrasts show unthresholded statistical comparisons with baseline period for each stage of the reaching task.

trajectories were adapted for small targets. These results show that high cue uncertainty and high target precision modulate all subjects' reaching kinematics, with ET patients making a slower movement

overall and showing more variation in velocity in response to changes in motor demand, relative to controls. We return to this in Section 3.7 where we analyse the low dimensional network dynamics that can explain these factors.

3.2 Analysis of Upper Limb Tremor

Upper-limb tremor amplitude was estimated from accelerometery (Supplementary Figure 2). ET patients on average exhibited a 0.85 ± 0.98 m/s^2 increase in tremor amplitude from rest to postural raise (paired t-test (10); t-statistic = 4.69; $P < 0.001$) at an average frequency of 5.8 ± 1.6 Hz. In 4/12 patients, a small (> 0.1 m/s^2) rest tremor was also present. In control subjects, the postural raise induced physiological tremor, but to a smaller extent of ~0.19 ± 0.04 m/s^2 (paired t-test (10); t-statistic = 7.06; $P < 0.001$). For reference, acceleration thresholds for visual detection of tremor by a subject or an observer are ~0.07m/s^2 [64]. Postural tremor amplitude positively correlated with clinical scoring (TETRAS performance subscale; Spearman's (12); R = 0.75; P = 0.010). There was no significant effect of cue uncertainty or target size on the tremor amplitude as evaluated at either motor preparation or at the hold period (Supplementary Figure 3).

3.3 Cortical Sources are Synchronized to Peripheral Tremor Rhythms

Sources in the brain that were synchronized to peripheral tremor were localized with a DICS beamformer. 75% of ET patients exhibited a peak in coherence (4-12 Hz, magnitude > 90th percentile of whole brain) over the cSMA (Figure 2A and B, EEG and OPM, respectively). cSMA EEG to accelerometer tremor coherence significantly increased in ET patients compared to controls (Figure 2C; peak t-statistic (10) = 2.24) and OPM recordings (Figure 2D; peak t-statistic (3) = 3.50). A subset of patients also exhibited coherence with tremor in the contralateral dorsolateral prefrontal cortex (dlPFC; 5/12 EEG patients, 2/4 OPM patients) that was significantly increased in ET relative to controls in the EEG data (Figure 2C). 3/4 of OPM patients exhibited a second tremor source in the contralateral posterior parietal cortex (cPPC) that was significantly increased in ET relative to controls (Figures 2D).

Due to the high coherence found in the cSMA, we performed an auxiliary DICS analysis that maximised sensitivity to weaker sources by regressing out the cSMA signal and focusing on the top 50% of coherent trials. This revealed a tremor coherent source that spanned ipsilateral and contralateral lobule VI of the Cerebellum present in 8/11 EEG patients (Figure 2E), and significantly increased in ET patients versus controls (peak t-statistic (21) = 2.43). A third peak was found in dlPFC that was present in 4/4 patients studied with OPM (Figure 2F) and was comparable to that

found in the EEG patients in Figure 2C. There was limited overlap between sources – subjects tended to exclusively have peaks in the Cerebellum VI, cPPC, or dlPFC. When ET patients were split by these regions, no statistically significant differences were found with respect to kinematics (reaction time, average

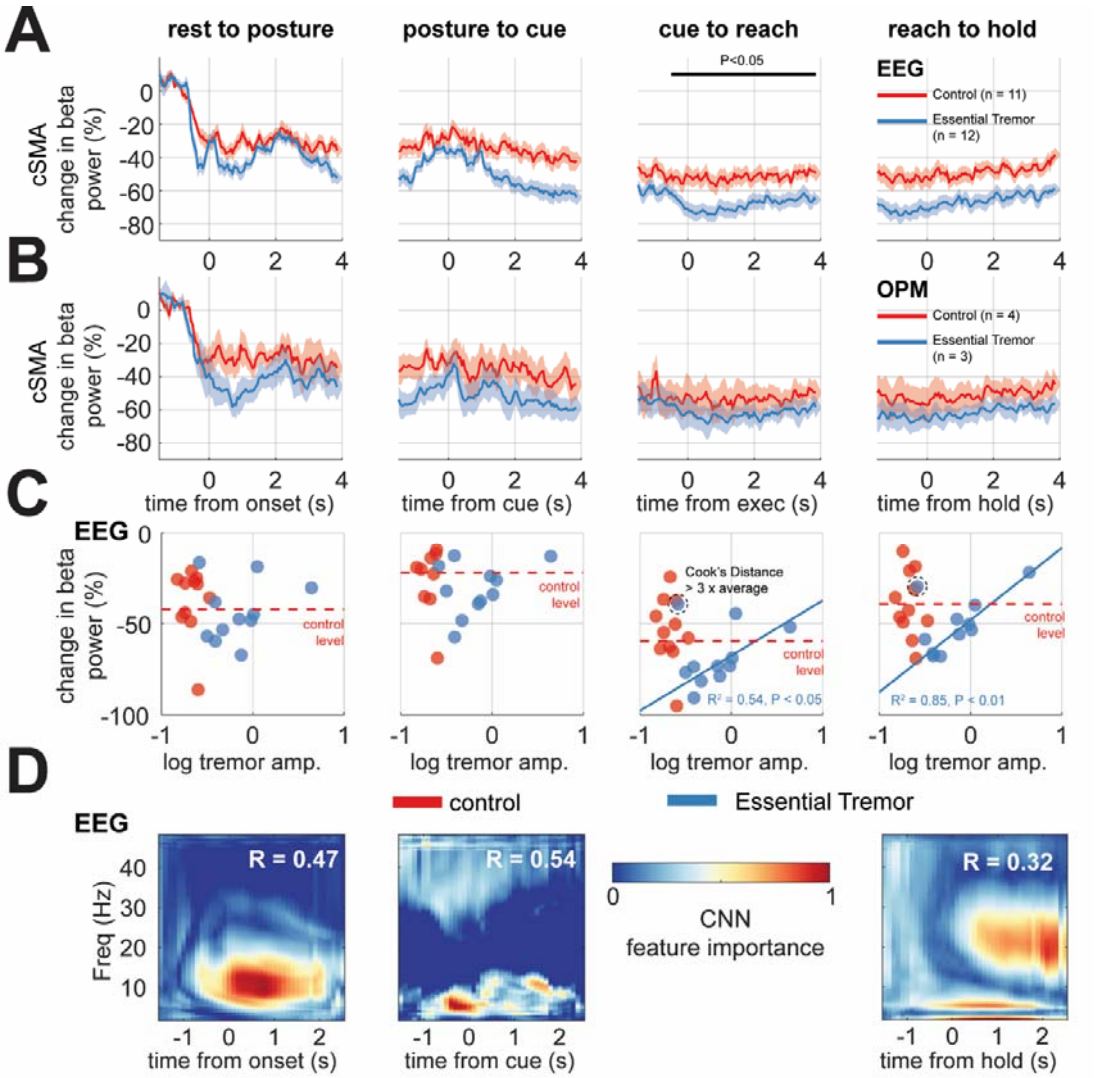

Figure 3 – Analysis comparing movement-induced beta event related desynchronization (ERD) in the contralateral supplementary motor area (cSMA) between Essential Tremor (ET) patients and Control recordings in EEG. (A) Time courses of low beta power (14-21 Hz) in the cSMA, scaled as the percentage change relative to at rest (0%), shown across the postural hold, reach planning, execution, and the hold period (columns left to right). Data is shown as the group average ±SEM, for controls (red) or ET patients (blue). Bars indicate significant decrease between controls and ETs, determined by one-sided cluster permutation statistics ($P < 0.05$). **(B)** Same as (A), but for OPM data. **(C)** Scatter plots of log scaled tremor amplitude versus the percentage change in beta power. Blue bold lines indicate the presence of a significant Pearson correlation for ET data point and associated regression line. The circled point indicates the outlier removed from regression. **(D)** Plots of the Grad-CAM feature importance maps of the group averaged time-frequency data from cSMA when using a convolutional neural network to predict tremor. Inset text gives the accuracy of the prediction in terms of R^2. This analysis was performed also for the high beta band and alternative brain regions

(Supplementary Figure 7 and Supplementary Figure 8).

velocity, or path length; ANOVA (11); $P > 0.05$) although the cerebellar group tended to have more severe tremor, but this did not pass significance (two-sample t-test (8), t-statistic = 1.27; $P > 0.05$).

These results show that the cSMA, cPPC, dlPFC and Cerebellum VI can become synchronized to tremor and are consistent with previous reports[25,26,28]. Importantly, these brain areas overlap with those involved in upper limb reaching[37,65]. This is confirmed by our analyses of time locked, motor induced activity that localized movement related beta synchronization[38] to the SMA in both OPM and EEG data and in control and tremor subjects (Figure 2G and H). In the following sections, we will investigate how pathological synchronization at tremor frequencies impacts neurophysiological signals associated with healthy motor processing.

3.4 Essential Tremor Patients Exhibit Deeper Movement Responsive Beta Desynchronization During Reaching

To investigate whether ET pathophysiology impacts physiological signals associated with motor processing, we focused on the activity in the cSMA, as this brain area is both synchronized to tremor frequencies and motor responsive (Section 3.3). Relative to controls, ET patients show a 15% increase (relative to at rest) in beta ERD in cSMA (Figure 3A) during reach execution and the post-movement hold period (one-sided t-test, permutation statistic (21), both $P < 0.05$). This effect was frequency and region specific, with no difference found for the upper beta band (21-30 Hz), nor in the cPPC, dlPFC, or ipsilateral Cerebellum VI (Supplementary Figure 7). ET patients studied with OPM also exhibited greater movement-related low beta frequency ERD to controls (Figure 3B), although this did not reach statistical significance, likely due to the smaller sample size. These results agree with previous work finding increased motor related beta ERD in electrocorticography recorded in patients with ET[66,67]. The degree of cSMA beta desynchronization during reach execution and the post-movement hold period were both negatively correlated with tremor severity in EEG recorded from ET patients (Figure 3C; reaching: $R^2 = 0.54$, $P < 0.05$ and hold: $R^2 = 0.85$, $P < 0.01$; 1 outlier removed on Cook's distance).

Finally, to predict patients' average tremor severity we applied a CNN to wide band (2-98 Hz) time-frequency spectrograms. A maximum tremor prediction accuracy of 25% (in terms of R^2) at the group level was achieved when using data taken from the cPPC (Appendix VII, table 1). Both cPPC and cSMA, were the most informative regions for the prediction of tremor severity. The Grad-CAM feature importances (Figure 3D) found power within the lower beta band at posture, theta (4-8 Hz) at planning stage, and higher beta band at the hold as being most predictive of tremor severity. OPM data yielded an average 5% improvement in tremor prediction compared to EEG (Appendix VIII, table 1).

These findings suggest that increased neural desynchrony in ET may form a compensatory mechanism to allow movement in patients, an idea we will return to in the

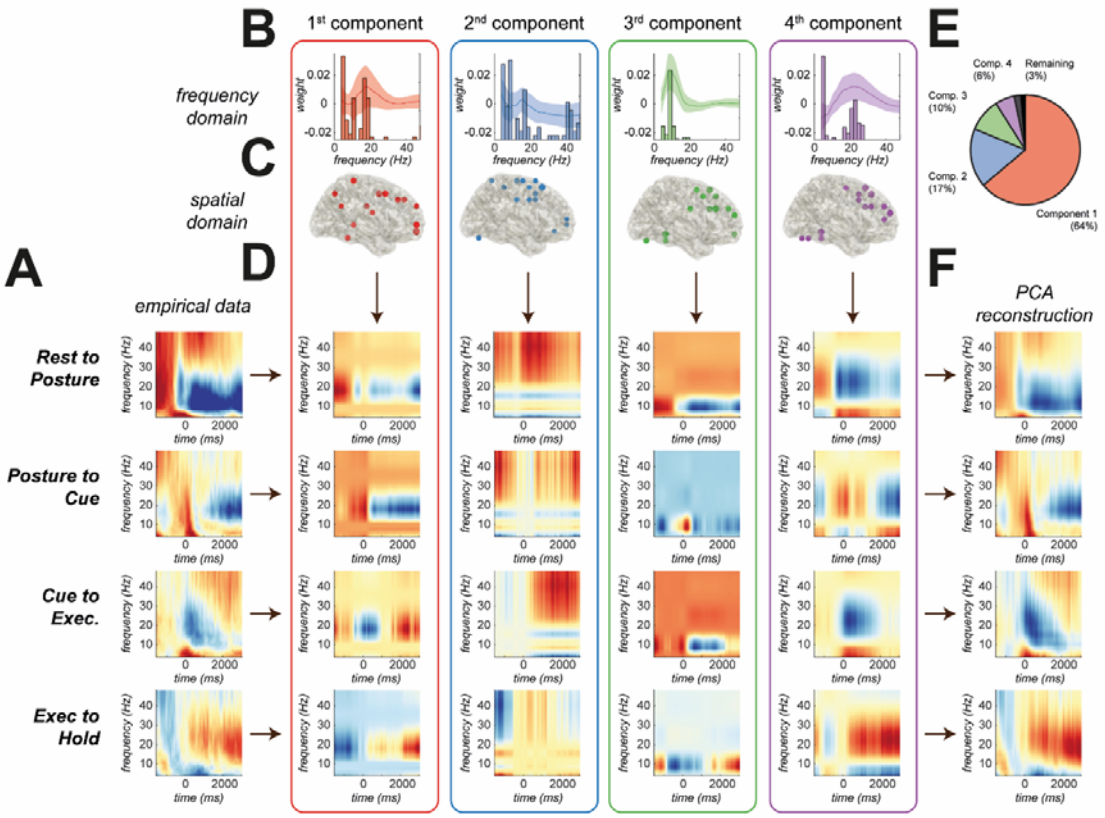

Figure 4 – Identification of large-scale, movement responsive brain circuits using time-frequency principal component analysis (tfPCA) applied to group averaged data (both ET and controls) derived from source-space projected EEG virtual electrodes. (A) Time-frequency spectrograms were computed for each region of interest (ROI) in the network, incorporating the dorsal prefrontal cortex, primary and supplementary motor areas, posterior parietal cortex, and cerebellum VI. tfPCA was applied to the group averaged EEG data, with spectrograms concatenated for each motor epoch. Prior to tfPCA, data was log scaled, and Z-normalized per subject. Visualization of the coefficients of each PCA component 1-4 (red, blue, green, and purple, respectively) in both the **(B)** frequency domain, and **(C)** spatial domain. **(D)** Back projection of empirical data allows for visualisation of the time-frequency dynamics of each component (averaged in space), across the four different epochs of the reaching task (corresponding to the rows). **(E)** Explained variance of the data by the four components. **(F)** Reconstruction of the original time-frequency data using the four components.

discussion. In section 3.8, we also analyse how these beta band signals relate to kinematics and tremor.

3.5 Time-Frequency Principal Component Analysis Identifies Known Motor Circuits

We now broaden our analysis to include signals across the wider brain and examined to what extent changes to activity in the cSMA represent wider changes across whole brain networks found in ET

and controls. We used tfPCA to reduce time-frequency descriptions of M/EEG source activity distributed

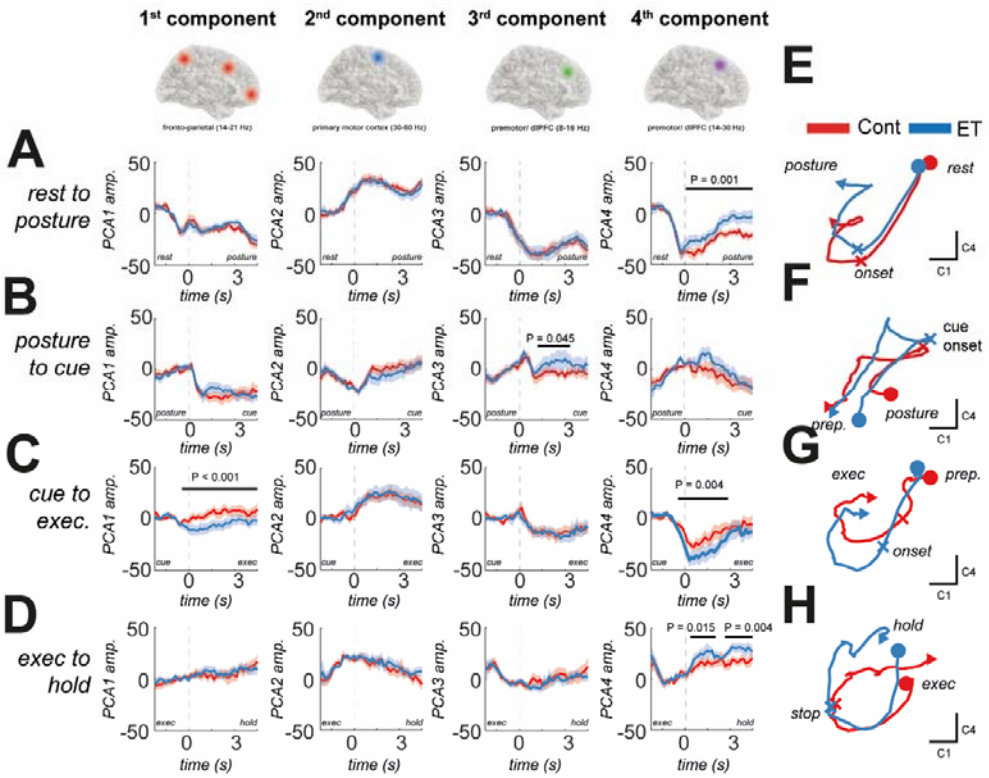

Figure 5 – Visualization of motor responsive, latent circuit dynamics and a comparison between controls and patients with ET recorded with EEG. Components were computed using tfPCA applied to the group averaged EEG data (Figure 4). These coefficients were then used to project data to trial-level latent dynamics that could be used to explore differences between controls and ET patients. **(A)** The latent dynamics exhibited during the postural hold for each component (columns) are plot for ET (blue) and controls (red) separately. Bars and associated P-values indicate the outcome of cluster permutation statistics between the two experimental groups. **(B-D)** Same as (A) but for cue presentation, reach execution, and the sustained hold. **(E-H)** Plots of the 2D latent trajectories (components 1 and 4, only) indicate highly correlated dynamics between controls and ETs with quantitative differences in the weighting of the components such as increased engagement of the prefrontal beta network in ET subjects (4th component, apparent in plot G). An equivalent analysis was performed for OPM recordings (Supplementary Figure 9).

across the brain into ensembles (c.f., components) characterized by distinct spatial and oscillatory characteristics.

Application of tfPCA to the group averaged EEG data (all ET and control subjects) identified four components that explain 97% of the total variance (Figure 4A and B) and accurately reconstructed the original data (Figure 4E). These components can be visualized in the original time-frequency space via back-projection (Figure 4D) or represented via their latent time dynamics (Figure 5). Component (1) is a fronto-parietal-sensorimotor network active in the lower beta band (14-21 Hz) and

desynchronises in preparation of movement (64% of total variance); Component (2) covering primary motor/somatosensory cortex that exhibits movement locked high frequency gamma activity (> 30 Hz; 17% of the total variance); Component (3) is a premotor/dorsolateral prefrontal network active at mu/beta band (8-16 Hz) that desynchronises at the onset of movement (10% of total variance); and Component (4) is a premotor/dorsolateral prefrontal network active across the beta band (14-30 Hz) that desynchronizes at movement onset (6% of the total variance).

3.6 Essential Tremor Patients Exhibit Differences in Large-Scale Circuit Dynamics

Using the tfPCA loadings computed at the group level we reconstructed the trial-level latent dynamics for each subject (Figure 5A) and examined differences between cohorts. The trajectories of latent dynamics were correlated between the controls and ET subjects (Figure 5E), with average between subject Pearson's correlation coefficients of R = 0.91 and R = 0.84 for EEG and OPM, respectively (Appendix IX, table 1). Latent dynamics were also highly preserved between EEG and OPM modalities (Supplementary Figure 9), with an average correlation coefficient of R = 0.73 (Appendix IX, table 2). ET participants exhibited a larger weighting of frontal-parietal low beta component (1st component) during reach execution (EEG patients only, Figure 5C; permutation t-statistic (74), $P < 0.001$). Both OPM and EEG data exhibited wide-band beta (14-30 Hz) ERD in the dorsolateral prefrontal beta network (4th component) that was increased during reach execution in ET relative to controls (Figure 5C; EEG permutation t-statistic (74), P = 0.004), followed by a stronger rebound during the post-movement hold period (Figure 5D; EEG permutation t-statistic (74), P = 0.004).

When using the M/EEG trial-projected time-frequency images from each component to predict tremor (Appendix VII and VIII; Tables 3 and 4), no increase in the CNN's accuracy was seen over that of the simpler region-specific analyses (Section 3.4). The 1st frontoparietal component was most predictive of tremor (average of $R^2 = 0.12$), and postural raise being the most informative epoch (average R^2 of 0.135). Within the subject, trial-by-trial prediction was not improved beyond the single region analyses (overall average $R^2 = 0.013$). The limited increase in tremor prediction from ensemble activity suggests that the information about tremor in the cSMA is sufficient to explain that across the whole network. This analysis of latent dynamics shows that the changes in cSMA found in ET patients (Section 3.4) is just one contributor to a wider network of motor regions altered by ET pathophysiology.

3.7 Whole Brain Latent Networks Can Explain Within-Subject Variation in Tremor and Kinematics

Finally, we explored whether the latent motor networks revealed by tfPCA could explain trial-by-trial variations in tremor severity (Figure 6). We used regression with a mixed GLM (Methods Section

2.11) as well statistical comparisons of data split between *low* and *high* trials of each kinematic (1st and 4th quartiles, respectively). High tremor severity during the hold period was associated with increased weighting of both the frontal-parietal low beta component (1st component; two-sided, paired t-statistic;

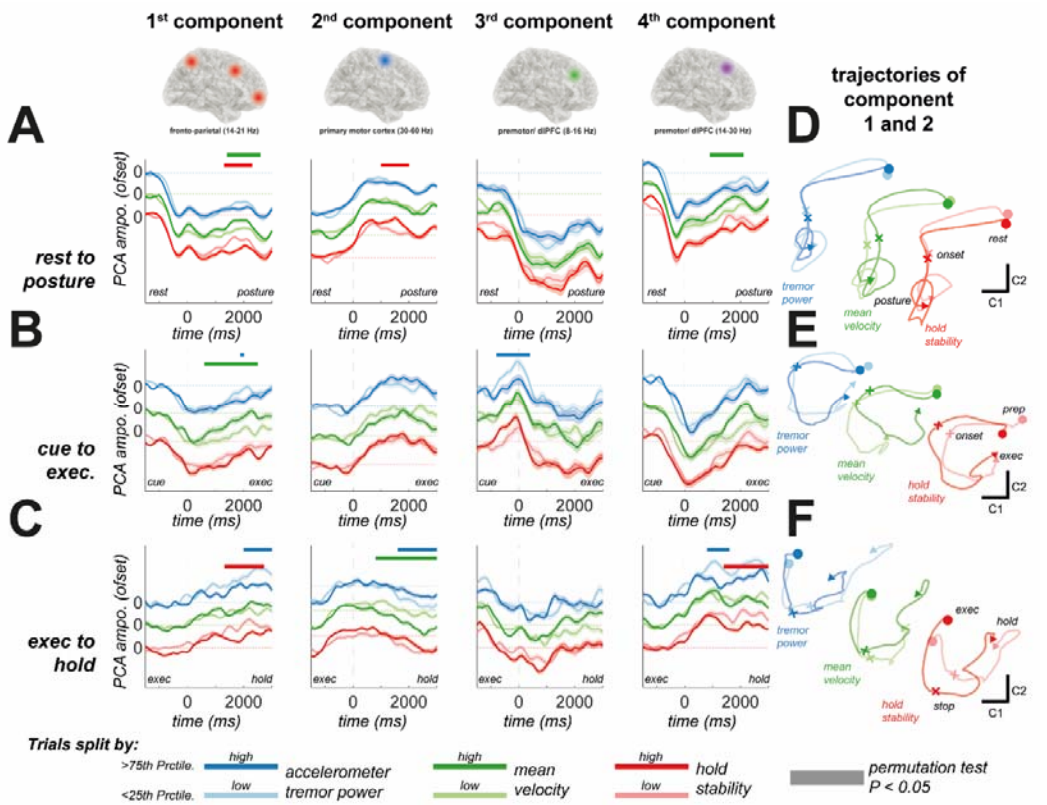

Figure 6 – Analysis of association between motor responsive latent circuit dynamics and movement kinematics over the task in the EEG subjects. Latent states were projected to the single trial level, using coefficients computed from group averaged time frequency EEG data. Differences in kinematic parameter are shown for both controls and ET patients, tremor parameters solely for ET patients. Trials were split into the 1st quartile (light colours) or 4th quartile (dark colours) and then compared at the group level using a cluster permutation test (indicated by thick lines). **(A)** Plots of the latent dynamics over the postural raise split by the tremor band power during each hold period (blue lines), the mean velocity during the postural raise/reach (green lines), and the stability of the hold period (red lines). Data is shown for the 1st, 2nd, 3rd, 4th PCA components (in respective columns). **(B-C)** Same as (A) but for movement execution phase and the hold phase, respectively. **(D-F)** 2D plots of the latent trajectories split by the kinematic features. Only components 1 and 2 are shown.

permutation t-statistic (11), $P < 0.01$) and premotor gamma component (2nd component; permutation t-statistic (11), $P < 0.05$). The 2nd component (high frequency 30-60 Hz oscillations over pre-motor regions) was consistently the most predictive of tremor severity across patients, with 40% of patients exhibiting significant within-subject correlations between this component's weighting and tremor amplitude.

In terms of reach kinematics, faster movement velocity in all subjects was associated with reduced frontoparietal beta power rebound (figure 6B; light green bars; 1st component; permutation t-statistic (22), $P < 0.01$). Increased hold stability (i.e., reduced variance of movement) at the hold periods was associated with slower rebound in both the frontoparietal beta network (1st component; light red bars; permutation t-statistic (21), $P < 0.001$) and the frontal beta network (4th component; light red bars; permutation t-statistic (21), $P < 0.01$). There was a high degree of overlap between time windows predictive of kinematics and tremor severity that may complicate their usage as control signals for closed loop neuromodulation. However, these results may help explain the findings of differences in latent dynamics between ET and controls (Section 3.7) and suggest that disturbance of frontal-parietal networks in ET may relate to differences in reaching kinematics seen in this task (Section 3.1).

4 Discussion

4.1 Summary of Results

The results here demonstrate that the pathophysiological changes in ET involve alterations of dynamics associated with large scale motor circuits during reaching. Patients can execute reaching movements with a similar degree of accuracy, but slower average velocity compared to controls (Figure 1). Regions such as cSMA, cPPC, dlPFC and Cereb. VI synchronize to inertial measures of tremor, but also show time locked beta oscillations in response to movement (Figure 2). The cSMA was synchronized to tremor in over 75% patients measured with EEG or OPM. Notably, we found that ET patients exhibited a 15% increase in movement responsive low beta ERD in cSMA during reaching, with a degree that inversely correlates with tremor severity (Figure 3). Changes in motor responsive theta and beta band oscillations could predict the average tremor magnitude of patients up to 25% variance explained. An analysis of whole brain activity using tfPCA revealed dynamics of four distinct oscillatory motor circuits that were well preserved across controls, patients and recording modalities (Figure 4). These analyses showed that changes in the cSMA were just part of a wider set of changes to frontoparietal and prefrontal circuits that were associated with ET (Figure 5). Latent dynamics of frontoparietal and premotor ensembles were able to predict trial level variability in tremor, albeit at a coarsely grained level. These features however were not well separated from those also predicting movement kinematics (Figure 6) - an important consideration if using these signals for control.

4.2 Informing Novel Strategies for Neurostimulation in Essential Tremor

This work builds upon previous reports that regions of the SMA, PPC, and Cerebellum are synchronized to peripheral tremor[25–27]. These regions relate to VL thalamic activity, which projects

extensively to these areas, is highly correlated with peripheral tremor signals[11,68,69], and is the primary target for DBS therapy in ET. Our analysis of source localized coherence from M/EEG neuroimaging strengthens evidence for a cerebro-cerebellar tremor network in ET. Regions such as the cerebellum or PPC may provide candidate sites for interruption of the tremor network with stimulation, as has recently been shown[15,33]. However, the overlap in representation of both tremor and kinematics in regions such as the

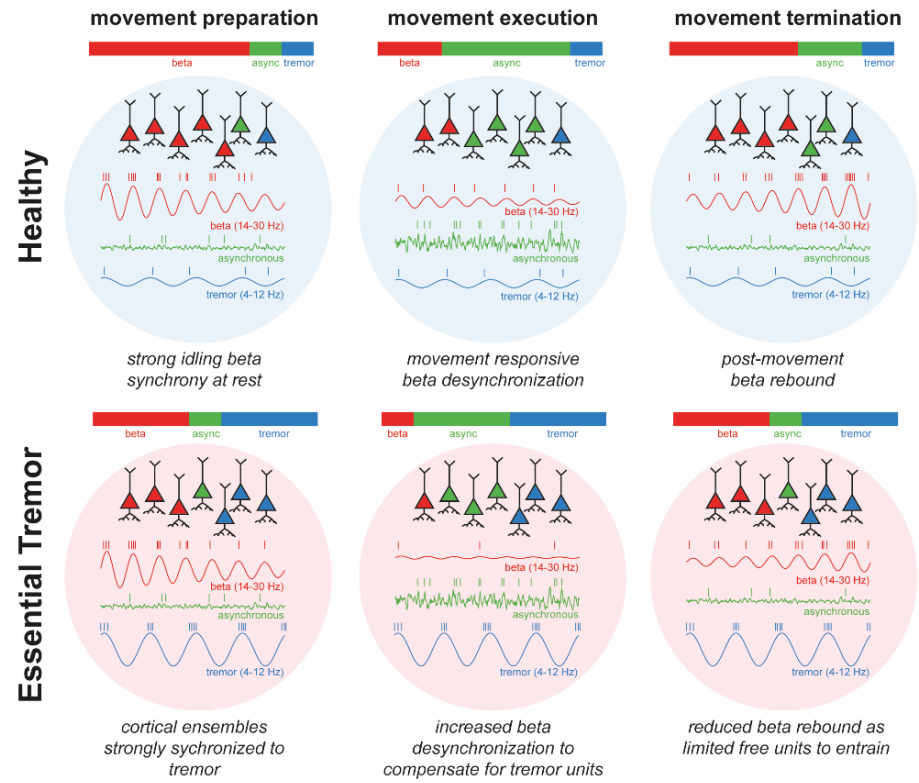

Figure 7 – Hypothetical mechanism that underlies compensatory motor related beta event related desynchronization (ERD) in patients with Essential Tremor. When the motor system is preparing to move (first column), populations of cortical neurons (here sketched as six individual units) are entrained to large scale brain rhythms such as the sensorimotor beta rhythm (shown in red), but also to tremor rhythms (blue). These can either be low amplitude 4-12 Hz oscillations at physiological tremor (i.e., in healthy participants, top row), or high amplitude pathological tremors associated with ET (bottom row). During movement (middle column), motor cortical neurons are known to exhibit firing rate changes (assumed here to be asynchronous; shown in green) that encode movement parameters. At the same time, ERD of the beta rhythm relinquishes units to participate in motor encoding. This is then followed by a post movement rebound of beta (final column). In ET (bottom row), the pathologically high amplitude tremor rhythm involves the entrainment of a higher fraction of cortical neurons reducing the effective information encoding capacity of the available pool of neurons. To compensate, during movement, there is an increased ERD of sensorimotor beta rhythms that frees up the neuronal "real estate" required to effectively encode movement.

primary or supplementary motor cortices, shows that whilst targeted stimulation has the potential to disrupt tremor[29,70], it may also impact the normal execution of movements[71].

Practically, cortical sensing could be used to control DBS, as has been done for Parkinson's disease[72], delivering thalamic stimulation proportional to expected tremor levels and considering motor context to provide state-dependent neuromodulation of ET[73,74]. Oscillatory signals associated with movement have been used previously for closed loop control of stimulation[40,41,75]. However, our results show that the inverse correlation of movement locked beta ERD with tremor amplitude may impede the detection of this signal in patients with the most severe tremors.

Going beyond the single region, we have shown ensemble activity in both fronto-parietal and premotor circuits can predict tremor severity (Figure 6) when split into low and high amplitude. Our results support the potential for multisite sensing in closed-loop neuromodulation [76,77], and specifically the ability for dimensionality reduction apporoaches such as tfPCA, to improve decoding of motor states [51,78]. Future application of supervised methods for dimensionality reduction are likely to improve this further by focusing latent dynamics on context relevant signals[79,80]. Using these simplified, low dimensional representations to predict tremor severity, could enable proportional controllers for DBS, as has proven effective in DBS for Parkinson's disease[82].

4.3 Functional Significance of Altered Motor Responsive Oscillations in ET

Movement responsive neural oscillations in the healthy brain[38,83,84] reflect important steps of sensorimotor processing[85]. Our finding of increased beta ERD in essential tremor (ET) suggests that tremor engages mechanisms similar to intentional movement, and may reflect compensatory activity to mitigate the effects of tremor. Interpretations of sensorimotor beta as an idling signal[86] suggest that increased beta ERD reflects the freeing up of cortical neurons to encode useful parameters of movement[87], and compensate for extraneous entrainment at the tremor rhythm (illustrated in Figure 7). Notably, the differences in beta ERD observed in ET were most apparent during the goal directed reach and not during the more stereotyped postural raise, suggesting increased complexity of the reaching movement demands greater mobilization of motor cortical resources, a finding in agreement with recent work showing that beta ERD scales with movement effort[88].

Recent findings also suggest that sensorimotor beta synchronization reflects sensory processing [89–92], such as when attenuating highly uncertain sensations[93]. In ET, it is likely that cerebellar deficits may introduce susceptibility to sensorimotor noise[94,95] that may drive a compensatory suppression of sensory information following movement, observable as an enhanced post-movement beta rebound in our data (Figure 5D). The intrusion of tremor into the reaching movement (i.e., dysmetria) may also explain the slowed beta rebound that we observed post movement. This accords with findings that

online control of movement is impaired in ET [96], and that therapeutic effects from thalamic DBS may arise from a "functional deafferentation" to attenuate sensory gain[97]. In the reaching task here, we observed a decrease in average movement velocity in ET patients, again suggesting an increased reliance on internal motor models. Our observations of effects across large-scale networks raise the question of whether DBS for ET can restore altered movement processing and associated signals, as has been investigated in Parkinson's disease[98]. Previous modelling work has shown that patterning of stimulation can be tuned to achieve specific network states[73], suggesting the potential for adaptive stimulation to steer compensatory motor activity in ET.

4.4 Application of Optically Pumped Magnetometry in Essential Tremor

The data presented here provides proof of principle for the deployment of non-cryogenic MEG enabled by OPM arrays to the study of naturalistic movement and movement disorders. Our results were validated by those signatures found with HD-EEG, with additional sensitivity to higher frequency, gamma rhythms[48] during reaching movement (Supplementary Figure 6) and small increases in tremor prediction with OPM (Section 3.4). Our analyses did not find clear evidence for cerebellar activations in OPM[99], although this could be explained by differences in the pathophysiology of the two cohorts, as well as suboptimal sensor cabling for detection in these recordings. We did however find that effect sizes of source localized power changes during parts of the task containing whole limb movements were markedly higher than for EEG (Appendix X), indicating more robust single subject estimates in OPM data. Finally, recent developments in corticospinal imaging with OPM[100,101] may allow for future studies to investigate the role of spinal afferents in the genesis of Essential Tremor.

4.5 Limitations

Identification of tremor synchronized sources depends upon coherence, a linear measure of oscillatory coupling. Due to this, analyses such as DICS used here, may be blind to remaining elements of the tremor circuit by ignoring nonlinear activity such as phase-amplitude coupling, known to be altered in ET[66]. This work has investigated whole limb naturalistic movements and faces the well-recognised challenges of motion-related artefacts arising from either contamination by myographic artefact and cable noise. Measurement of tremor during large movements is challenging, due to shifts in the tremor axis and gravity artefacts, which could be reduced through the usage of gyroscope estimates in future studies. It should be noted that there was no explicit forward model of the cerebellum, inclusion of which is likely to significantly improve cerebellar localization[102]

4.6 Conclusions

This study reveals that large-scale oscillatory networks required for whole limb movement control are significantly disrupted by ET pathophysiology. MEEG analysis shows ET patients exhibit heightened movement-related beta ERD, particularly in the cSMA, compared to controls. We propose this desynchronization compensates for neural resources otherwise entrained at tremor frequencies, to enable normal motor control. Novel dimensionality reduction analysis supports this further, pinpointing disruptions in a distributed tremor network involving the SMA, PPC, dlPFC, and Cerebellum VI, regions all involved in volitional motor control. Disturbances in fronto-parietal and premotor processing during reaching movements predict tremor severity and overlap with kinematic encoding, indicating a relationship between these processes. These findings enhance our understanding of ET pathophysiology's impact on motor control signals and identify targets for developing future non-invasive, context-responsive neuromodulation approaches.

5 Data Availability

Upon publication, the anonymised source reconstructed data and the code required to reproduce the analyses in this report will be shared to a publicly available repository on Zenodo with version control.

6 Acknowledgements

We extend our thanks to the UCL OPM development team for making these recordings possible; Carolina Reis for help with early testing; the authors who develop, maintain, and freely share several toolboxes (listed in Appendix XI); Alto Neuroimaging at Aalto University for providing the accelerometer system used in the OPM experiments; and the anonymous participants who generously gave up their time to take part in this study.

7 Funding

SF Acknowledges philanthropic funding support from Moger Moves, Paddy and Jacky Sellers and Szeben-Peto donations. AC was supported by a travel grant from the Prof. Klaus Thiemann foundation. BW conducted his work with the support of the Erasmus+ programme of the European Union. HC, TW were supported by the Medical Research Council UK Award (MR/R020418/1; MR/X023141/1); the Wellcome Institutional Strategic Support Fund (204826/Z/16/Z). The Wellcome Centre for Human Neuroimaging is supported by core funding from Wellcome (203147/Z/16/Z).

8 Competing Interests

T.S. provides paid consultancy for Jazz Pharmaceuticals. The remaining authors have no competing interests to declare. The European Commission support for the production of this publication does not constitute an endorsement of the contents which reflects the views only of the authors, and the Commission cannot be held responsible for any use which may be made of the information contained therein.

9 References

1. Elble RJ, Deuschl G. An update on essential tremor. *Curr Neurol Neurosci Rep*. 2009;9(4):273-277. doi:10.1007/s11910-009-0041-6

2. Thanvi B, Lo N, Robinson T. Essential tremor—the most common movement disorder in older people. *Age Ageing*. 2006;35(4):344-349. doi:10.1093/AGEING/AFJ072

3. Rohani M, Fasano A. Focused Ultrasound for Essential Tremor: Review of the Evidence and Discussion of Current Hurdles. *Tremor and Other Hyperkinetic Movements*. 2017;7. doi:10.7916/D8Z89JN1

4. Shih LC, LaFaver K, Lim C, Papavassiliou E, Tarsy D. Loss of benefit in VIM thalamic deep brain stimulation (DBS) for essential tremor(ET): How prevalent is it? *Parkinsonism Relat Disord*. 2013;19(7):676-679. doi:10.1016/j.parkreldis.2013.03.006

5. Barbe MT, Liebhart L, Runge M, et al. Deep brain stimulation in the nucleus ventralis intermedius in patients with essential tremor: Habituation of tremor suppression. *J Neurol*. 2011;258(3):434-439. doi:10.1007/s00415-010-5773-3

6. Hedera P. Emerging strategies in the management of essential tremor. *Ther Adv Neurol Disord*. 2017;10(2):137-148. doi:10.1177/1756285616679123

7. Isaacson SH, Peckham E, Tse W, et al. Prospective Home-use Study on Non-invasive Neuromodulation Therapy for Essential Tremor. *Tremor Other Hyperkinet Mov (N Y)*. 2020;10(1):1-16. doi:10.5334/TOHM.59

8. Kim J, Wichmann T, Inan OT, Deweerth SP. A Wearable System for Attenuating Essential Tremor Based on Peripheral Nerve Stimulation. *IEEE J Transl Eng Health Med*. 2020;8. doi:10.1109/JTEHM.2020.2985058

9. Dideriksen JL, Laine CM, Dosen S, et al. Electrical Stimulation of Afferent Pathways for the Suppression of Pathological Tremor. *Front Neurosci*. 2017;11(APR). doi:10.3389/FNINS.2017.00178

10. Gallego JÁ, Rocon E, Belda-Lois JM, Pons JL. A neuroprosthesis for tremor management through the control of muscle co-contraction. *J Neuroeng Rehabil*. 2013;10(1). doi:10.1186/1743-0003-10-36

11. Pedrosa DJ, Brown P, Cagnan H, et al. A functional micro-electrode mapping of ventral thalamus in essential tremor. *Brain*. 2018;141(9):2644-2654. doi:10.1093/brain/awy192

12. Reis C, Arruda BS, Pogosyan A, Brown P, Cagnan H. Essential tremor amplitude modulation by median nerve stimulation. *Scientific Reports 2021 11:1*. 2021;11(1):1-10. doi:10.1038/s41598-021-96660-6

13. Cagnan H, Pedrosa D, Little S, et al. Stimulating at the right time: phase-specific deep brain stimulation. *Brain*. 2017;140(1):132-145. doi:10.1093/brain/aww286

14. Dosen S, Muceli S, Dideriksen JL, et al. Online tremor suppression using electromyography and low-level electrical stimulation. *IEEE Transactions on Neural Systems and Rehabilitation Engineering*. 2015;23(3):385-395. doi:10.1109/TNSRE.2014.2328296

15. Schreglmann SR, Wang D, Peach RL, et al. Non-invasive suppression of essential tremor via phase-locked disruption of its temporal coherence. *Nature Communications 2021 12:1*. 2021;12(1):1-15. doi:10.1038/s41467-020-20581-7

16. Cernera S, Alcantara JD, Opri E, et al. Wearable sensor-driven responsive deep brain stimulation for essential tremor. *Brain Stimul*. 2021;14(6):1434-1443. doi:10.1016/j.brs.2021.09.002

17. Sharifi S, Luft F, Verhagen R, et al. Intermittent cortical involvement in the preservation of tremor in essential tremor. *J Neurophysiol*. 2017;118(5):2628-2635. doi:10.1152/jn.00848.2016

18. Pedrosa DJ, Quatuor EL, Reck C, et al. Thalamomuscular coherence in essential tremor: hen or egg in the emergence of tremor? *J Neurosci*. 2014;34(43):14475-14483. doi:10.1523/JNEUROSCI.0087-14.2014

19. Raethjen J, Deuschl G. The oscillating central network of Essential tremor. *Clinical Neurophysiology*. 2012;123(1):61-64. doi:10.1016/j.clinph.2011.09.024

20. Helmich RC, Toni I, Deuschl G, Bloem BR. The pathophysiology of essential tremor and parkinson's tremor. *Curr Neurol Neurosci Rep*. 2013;13(9):1-10. doi:10.1007/s11910-013-0378-8

21. Gallea C, Popa T, García-Lorenzo D, et al. Intrinsic signature of essential tremor in the cerebello-frontal network. *Brain*. 2015;138(10):2920-2933. doi:10.1093/brain/awv171

22. Archer DB, Coombes SA, Chu WT, et al. A widespread visually-sensitive functional network relates to symptoms in essential tremor. *Brain*. 2018;141(2):472-485. doi:10.1093/brain/awx338

23. Boscolo Galazzo I, Magrinelli F, Pizzini FB, et al. Voxel-based morphometry and task functional magnetic resonance imaging in essential tremor: evidence for a disrupted brain network. *Sci Rep*. 2020;10(1):1-14. doi:10.1038/s41598-020-69514-w

24. Buijink AWG, Broersma M, van der Stouwe AMM, et al. Rhythmic finger tapping reveals cerebellar dysfunction in essential tremor. *Parkinsonism Relat Disord*. 2015;21(4):383-388. doi:10.1016/j.parkreldis.2015.02.003

25. Muthuraman M, Raethjen J, Koirala N, et al. Cerebello-cortical network fingerprints differ between essential, Parkinson's and mimicked tremors. *Brain*. 2018;141(6):1770-1781. doi:10.1093/brain/awy098

26. Raethjen J, Govindan RB, Kopper F, Muthuraman M, Deuschl G. Cortical involvement in the generation of essential tremor. *J Neurophysiol*. 2007;97(5):3219-3228. doi:10.1152/jn.00477.2006

27. Pedrosa DJ, Nelles C, Brown P, et al. The differentiated networks related to essential tremor onset and its amplitude modulation after alcohol intake. *Exp Neurol*. 2017;297:50-61. doi:10.1016/j.expneurol.2017.07.013

28. Schnitzler A, Münks C, Butz M, Timmermann L, Gross J. Synchronized brain network associated with essential tremor as revealed by magnetoencephalography. *Movement Disorders*. 2009;24(11):1629-1635. doi:10.1002/mds.22633

29. Hellriegel H, Schulz EM, Siebner HR, Deuschl G, Raethjen JH. Continuous theta-burst stimulation of the primary motor cortex in essential tremor. *Clinical Neurophysiology*. 2012;123(5):1010-1015. doi:10.1016/J.CLINPH.2011.08.033

30. Brittain JS, Probert-Smith P, Aziz TZ, Brown P. Tremor suppression by rhythmic transcranial current stimulation. *Current Biology*. 2013;23(5):436-440. doi:10.1016/j.cub.2013.01.068

31. Popa T, Russo M, Vidailhet M, et al. Cerebellar rTMS stimulation may induce prolonged clinical benefits in essential tremor, and subjacent changes in functional connectivity: An open label trial. *Brain Stimul*. 2013;6(2):175-179. doi:10.1016/J.BRS.2012.04.009

32. Bologna M, Rocchi L, Leodori G, et al. Cerebellar Continuous Theta Burst Stimulation in Essential Tremor. *Cerebellum*. 2015;14(2):133-141. doi:10.1007/S12311-014-0621-0/FIGURES/4

33. Olivier C, Lamy JC, Kosutzka Z, et al. Cerebellar Transcranial Alternating Current Stimulation in Essential Tremor Patients with Thalamic Stimulation: A Proof-of-Concept Study. *Neurotherapeutics*. 2023;20(4):1109-1119. doi:10.1007/S13311-023-01372-6

34. Hammond C, Bergman H, Brown P. Pathological synchronization in Parkinson's disease: networks, models and treatments. *Trends Neurosci*. 2007;30(7):357-364. doi:10.1016/j.tins.2007.05.004

35. Stam CJ. Modern network science of neurological disorders. *Nat Rev Neurosci*. 2014;15(10):683-695. doi:10.1038/nrn3801

36. Inagaki HK, Chen S, Daie K, et al. Neural Algorithms and Circuits for Motor Planning. *https://doi.org/101146/annurev-neuro-092021-121730*. 2022;45(1). doi:10.1146/ANNUREV-NEURO-092021-121730

37. Haggard P. Conscious intention and motor cognition. *Trends Cogn Sci*. 2005;9(6):290-295. doi:10.1016/j.tics.2005.04.012

38. Pfurtscheller G, Lopes da Silva FH. Event-related EEG/MEG synchronization and desynchronization: basic principles. *Clinical Neurophysiology*. 1999;110(11):1842-1857. doi:10.1016/S1388-2457(99)00141-8

39. Herron JA, Thompson MC, Brown T, Chizeck HJ, Ojemann JG, Ko AL. Chronic electrocorticography for sensing movement intention and closed-loop deep brain stimulation with wearable sensors in an essential tremor patient. *J Neurosurg*. 2017;127(3):580-587. doi:10.3171/2016.8.JNS16536

40. He S, Baig F, Mostofi A, et al. Closed□Loop Deep Brain Stimulation for Essential Tremor Based on Thalamic Local Field Potentials. *Movement Disorders*. 2021;36(4):863-873. doi:10.1002/mds.28513

41. Opri E, Cernera S, Molina R, et al. Chronic embedded cortico-thalamic closed-loop deep brain stimulation for the treatment of essential tremor. *Sci Transl Med*. 2020;12(572). doi:10.1126/SCITRANSLMED.AAY7680

42. Farkas Z, Szirmai I, Kamondi A. Impaired rhythm generation in essential tremor. *Mov Disord*. 2006;21(8):1196-1199. doi:10.1002/MDS.20934

43. Köster B, Deuschl G, Lauk M, Timmer J, Guschlbauer B, Lücking CH. Essential tremor and cerebellar dysfunction: abnormal ballistic movements. *J Neurol Neurosurg Psychiatry*. 2002;73(4):400. doi:10.1136/JNNP.73.4.400

44. Britton TC, Thompson PD, Day BL, Rothwell JC, Findley LJ, Marsden CD. Rapid wrist movements in patients with essential tremor. The critical role of the second agonist burst. *Brain*. 1994;117 (Pt 1)(1):39-47. doi:10.1093/BRAIN/117.1.39

45. Boto E, Holmes N, Leggett J, et al. Moving magnetoencephalography towards real-world applications with a wearable system. *Nature*. 2018;555(7698):657-661. doi:10.1038/nature26147

46. Seymour RA, Alexander N, Mellor S, et al. Using OPMs to measure neural activity in standing, mobile participants. *Neuroimage*. 2021;244:118604. doi:10.1016/j.neuroimage.2021.118604

47. Roberts G, Holmes N, Alexander N, et al. Towards OPM-MEG in a virtual reality environment. *Neuroimage*. 2019;199:408-417. doi:10.1016/j.neuroimage.2019.06.010

48. Hill RM, Schofield H, Boto E, et al. Optimising the sensitivity of optically-pumped magnetometer magnetoencephalography to gamma band electrophysiological activity. *Imaging Neuroscience*. 2024;2:1-19. doi:10.1162/imag_a_00112

49. Bernat EM, Williams WJ, Gehring WJ. Decomposing ERP time-frequency energy using PCA. *Clinical Neurophysiology*. 2005;116(6):1314-1334. doi:10.1016/j.clinph.2005.01.019

50. Kao JC, Nuyujukian P, Ryu SI, Churchland MM, Cunningham JP, Shenoy K V. Single-trial dynamics of motor cortex and their applications to brain-machine interfaces. *Nature Communications 2015 6:1*. 2015;6(1):1-12. doi:10.1038/ncomms8759

51. Yang Y, Qiao S, Sani OG, et al. Modelling and prediction of the dynamic responses of large-scale brain networks during direct electrical stimulation. *Nat Biomed Eng*. 2021;5(4):324-345. doi:10.1038/s41551-020-00666-w

52. John YJ, Sawyer KS, Srinivasan K, Müller EJ, Munn BR, Shine JM. It’s about time: Linking dynamical systems with human neuroimaging to understand the brain. *Network Neuroscience*. 2022;6(4):960-979. doi:10.1162/NETN_A_00230

53. Song H, Shim WM, Rosenberg MD. Large-scale neural dynamics in a shared low-dimensional state space reflect cognitive and attentional dynamics. *Elife*. 2023;12. doi:10.7554/ELIFE.85487

54. Thiery T, Rainville P, Cisek P, Jerbi K. Distinct trajectories in low-dimensional neural oscillation state space track dynamic decision-making in humans. *bioRxiv*. Published online June 16, 2022:2022.06.14.494674. doi:10.1101/2022.06.14.494674

55. Bhatia KP, Bain P, Bajaj N, et al. Consensus Statement on the classification of tremors. from the task force on tremor of the International Parkinson and Movement Disorder Society. *Mov Disord*. 2018;33(1):75-87. doi:10.1002/MDS.27121

56. Elble RJ. The essential tremor rating assessment scale. *J Neurol Neuromedicine*. 2016;1(4).

57. Oostenveld R, Fries P, Maris E, Schoffelen JM. FieldTrip: Open source software for advanced analysis of MEG, EEG, and invasive electrophysiological data. *Comput Intell Neurosci*. 2011;2011. doi:10.1155/2011/156869

58. Tierney TM, Alexander N, Mellor S, et al. Modelling optically pumped magnetometer interference in MEG as a spatially homogeneous magnetic field. *Neuroimage*. 2021;244:118484. doi:10.1016/j.neuroimage.2021.118484

59. Kutner MH, Neter J. *Applied Linear Regression Models*. McGraw-Hill/Irwin; 2004.

60. Gross J, Kujala J, Hamalainen M, Timmermann L, Schnitzler A, Salmelin R. Dynamic imaging of coherent sources: Studying neural interactions in the human brain. *Proc Natl Acad Sci U S A*. 2001;98(2):694-699. doi:10.1073/pnas.98.2.694

61. Bourguignon M, De Tiège X, de Beeck MO, et al. Functional motor-cortex mapping using corticokinematic coherence. *Neuroimage*. 2011;55(4):1475-1479. doi:10.1016/j.neuroimage.2011.01.031

62. Rolls ET, Huang CC, Lin CP, Feng J, Joliot M. Automated anatomical labelling atlas 3. *Neuroimage*. 2020;206:116189. doi:10.1016/j.neuroimage.2019.116189

63. Bokil H, Purpura K, Schoffelen JM, Thomson D, Mitra P. Comparing spectra and coherences for groups of unequal size. *J Neurosci Methods*. 2007;159(2):337-345. doi:10.1016/J.JNEUMETH.2006.07.011

64. Wade P, Gresty MA, Findley LJ. A Normative Study of Postural Tremor of the Hand. *Arch Neurol*. 1982;39(6):358-362. doi:10.1001/archneur.1982.00510180036009

65. Johnson PB, Ferraina S, Bianchi L, Caminiti R. Cortical Networks for Visual Reaching: Physiological and Anatomical Organization of Frontal and Parietal Lobe Arm Regions. *Cerebral Cortex*. 1996;6(2):102-119. doi:10.1093/cercor/6.2.102

66. Kondylis ED, Randazzo MJ, Alhourani A, et al. Movement-related dynamics of cortical oscillations in Parkinson's disease and essential tremor. *Brain*. 2016;139(8):2211-2223. doi:10.1093/brain/aww144

67. Crowell AL, Ryapolova-Webb ES, Ostrem JL, et al. Oscillations in sensorimotor cortex in movement disorders: an electrocorticography study. *Brain*. 2012;135(2):615-630. doi:10.1093/BRAIN/AWR332

68. Hua SE, Lenz FA, Zirh TA, Reich SG, Dougherty PM. Thalamic neuronal activity correlated with essential tremor. *J Neurol Neurosurg Psychiatry*. 1998;64(2):273-276. doi:10.1136/JNNP.64.2.273

69. Marsden JF, Ashby P, Limousin-Dowsey P, Rothwell JC, Brown P. Coherence between cerebellar thalamus, cortex and muscle in man. Cerebellar thalamus interactions. *Brain*. 2000;123(7):1459-1470. doi:10.1093/brain/123.7.1459

70. Brittain JS, Probert-Smith P, Aziz TZ, Brown P. Tremor Suppression by Rhythmic Transcranial Current Stimulation. *Current Biology*. 2013;23(5):436-440. doi:10.1016/J.CUB.2013.01.068

71. Gerloff C, Corwell B, Chen R, Hallett M, Cohen LG. Stimulation over the human supplementary motor area interferes with the organization of future elements in complex motor sequences. *Brain*. 1997;120(9):1587-1602. doi:10.1093/brain/120.9.1587

72. Swann NC, de Hemptinne C, Thompson MC, et al. Adaptive deep brain stimulation for Parkinson's disease using motor cortex sensing. *J Neural Eng*. 2018;15(4):46006. doi:10.1088/1741-2552/aabc9b

73. West TO, Magill PJ, Sharott A, Litvak V, Farmer SF, Cagnan H. Stimulating at the right time to recover network states in a model of the cortico-basal ganglia-thalamic circuit. Rubin J, ed. *PLoS Comput Biol*. 2022;18(3):e1009887. doi:10.1371/journal.pcbi.1009887

74. Fleming JE, Pont Sanchis I, Lemmens O, et al. From dawn till dusk: Time-adaptive bayesian optimization for neurostimulation. Marinazzo D, ed. *PLoS Comput Biol*. 2023;19(12):e1011674. doi:10.1371/journal.pcbi.1011674

75. Herron JA, Thompson MC, Brown T, Chizeck HJ, Ojemann JG, Ko AL. Chronic electrocorticography for sensing movement intention and closed-loop deep brain stimulation with wearable sensors in an essential tremor patient. *J Neurosurg*. 2017;127(3):580-587. doi:10.3171/2016.8.JNS16536

76. Swann NC, Hemptinne C de, Miocinovic S, et al. Chronic multisite brain recordings from a totally implantable bidirectional neural interface: experience in 5 patients with Parkinson's disease. *Journal of Neurosurgery JNS*. 2017;128(2):605-616. doi:10.3171/2016.11.JNS161162

77. Muldoon SF, Pasqualetti F, Gu S, et al. Stimulation-Based Control of Dynamic Brain Networks. Hilgetag CC, ed. *PLoS Comput Biol*. 2016;12(9):e1005076. doi:10.1371/journal.pcbi.1005076

78. Wang NXR, Olson JD, Ojemann JG, Rao RPN, Brunton BW. Unsupervised Decoding of Long-Term, Naturalistic Human Neural Recordings with Automated Video and Audio Annotations. *Front Hum Neurosci*. 2016;10(APR2016):1-13. doi:10.3389/fnhum.2016.00165

79. Pandarinath C, O'Shea DJ, Collins J, et al. Inferring single-trial neural population dynamics using sequential auto-encoders. *Nat Methods*. 2018;15(10):805-815. doi:10.1038/s41592-018-0109-9

80. Brunton BW, Johnson LA, Ojemann JG, Kutz JN. Extracting spatial-temporal coherent patterns in large-scale neural recordings using dynamic mode decomposition. *J Neurosci Methods*. 2016;258:1-15. doi:10.1016/j.jneumeth.2015.10.010

81. Gu S, Pasqualetti F, Cieslak M, et al. Controllability of structural brain networks. *Nature Communications 2015 6:1*. 2015;6(1):1-10. doi:10.1038/ncomms9414

82. Schmidt SL, Chowdhury AH, Mitchell KT, et al. At home adaptive dual target deep brain stimulation in Parkinson's disease with proportional control. *Brain*. 2024;147(3):911-922. doi:10.1093/brain/awad429

83. Ramos-Murguialday A, Birbaumer N. Brain oscillatory signatures of motor tasks. *J Neurophysiol*. 2015;113(10):3663-3682. doi:10.1152/jn.00467.2013

84. Miller KJ, Leuthardt EC, Schalk G, et al. Spectral Changes in Cortical Surface Potentials during Motor Movement. *Journal of Neuroscience*. 2007;27(9):2424-2432. doi:10.1523/JNEUROSCI.3886-06.2007

85. Spitzer B, Haegens S. Beyond the status quo: A role for beta oscillations in endogenous content (RE)activation. *eNeuro*. 2017;4(4). doi:10.1523/ENEURO.0170-17.2017

86. Engel AK, Fries P. Beta-band oscillations—signalling the status quo? *Curr Opin Neurobiol*. 2010;20(2):156-165. doi:10.1016/j.conb.2010.02.015

87. Brittain JS, Sharott A, Brown P. The highs and lows of beta activity in cortico-basal ganglia loops. *European Journal of Neuroscience*. 2014;39(11):1951-1959. doi:10.1111/ejn.12574

88. Pierrieau E, Berret B, Lepage JF, Bernier PM. From Motivation to Action: Action Cost Better Predicts Changes in Premovement Beta-Band Activity than Speed. *Journal of Neuroscience*. 2023;43(28):5264-5275. doi:10.1523/JNEUROSCI.0213-23.2023

89. Mirzaei A, Kumar A, Leventhal D, et al. Sensorimotor Processing in the Basal Ganglia Leads to Transient Beta Oscillations during Behavior. *J Neurosci*. 2017;37(46):11220-11232. doi:10.1523/JNEUROSCI.1289-17.2017

90. Palmer CE, Auksztulewicz R, Ondobaka S, Kilner JM. Sensorimotor beta power reflects the precision-weighting afforded to sensory prediction errors. *Neuroimage*. 2019;200(June):59-71. doi:10.1016/j.neuroimage.2019.06.034

91. Karvat G, Alyahyay M, Diester I. Spontaneous activity competes with externally evoked responses in sensory cortex. *Proc Natl Acad Sci U S A*. 2021;118(25). doi:10.1073/pnas.2023286118

92. West TO, Duchet B, Farmer SF, Friston KJ, Cagnan H. When do Bursts Matter in the Primary Motor Cortex? Investigating Changes in the Intermittencies of Beta Rhythms Associated With Movement States. *Prog Neurobiol*. Published online December 21, 2023:102397. doi:10.1016/j.pneurobio.2022.102397

93. Tan H, Wade C, Brown P. Post-Movement Beta Activity in Sensorimotor Cortex Indexes Confidence in the Estimations from Internal Models. *Journal of Neuroscience*. 2016;36(5).

94. Lee RG, Stein RB. Resetting of tremor by mechanical perturbations: A comparison of essential tremor and parkinsonian tremor. *Ann Neurol*. 1981;10(6):523-531. doi:10.1002/ana.410100606

95. Elble RJ, Higgins C, Hughes L. Phase resetting and frequency entrainment of essential tremor. *Exp Neurol*. 1992;116(3):355-361. doi:10.1016/0014-4886(92)90014-H

96. Blondiaux F, Colmant L, Lebrun L, Hanseeuw B, Crevecoeur F. Erroneous compensation for long-latency feedback delays as origin of Essential Tremor. *bioRxiv*. Published online January 18, 2024:2024.01.11.575204. doi:10.1101/2024.01.11.575204

97. Anderson TR, Hu B, Iremonger K, Kiss ZHT. Selective attenuation of afferent synaptic transmission as a mechanism of thalamic deep brain stimulation-induced tremor arrest. *J Neurosci*. 2006;26(3):841-850. doi:10.1523/JNEUROSCI.3523-05.2006

98. Oswal A, Beudel M, Zrinzo L, et al. Deep brain stimulation modulates synchrony within spatially and spectrally distinct resting state networks in Parkinson's disease. *Brain*. 2016;139(5):1482-1496. doi:10.1093/brain/aww048

99. Lin CH, Tierney TM, Holmes N, et al. Using optically-pumped magnetometers to measure magnetoencephalographic signals in the human cerebellum. *bioRxiv*. Published online 2018:1-21. doi:10.1101/425447

100. Spedden M. Non-invasive evidence for rhythmic interactions between the human brain, spinal cord, and muscle. *bioRxiv*. Published online May 2, 2024:2024.05.01.591590. doi:10.1101/2024.05.01.591590

101. Mardell LC, Spedden ME, O'Neill GC, et al. Concurrent spinal and brain imaging with optically pumped magnetometers. *J Neurosci Methods*. 2024;406:110131. doi:10.1016/j.jneumeth.2024.110131

102. Andersen LM, Jerbi K, Dalal SS. Can EEG and MEG detect signals from the human cerebellum? *Neuroimage*. 2020;215. doi:10.1016/J.NEUROIMAGE.2020.116817

103. Nolte G. The magnetic lead field theorem in the quasi-static approximation and its use for magnetoenchephalography forward calculation in realistic volume conductors. *Phys Med Biol*. 2003;48(22):3637-3652. doi:10.1088/0031-9155/48/22/002

104. Westner BU, Dalal SS, Gramfort A, et al. A unified view on beamformers for M/EEG source reconstruction. *Neuroimage*. 2022;246:118789. doi:10.1016/j.neuroimage.2021.118789

10 Supplementary Figures

10.1 Supplementary Figure 1 – Convolutional Neural Network for Movement Detection

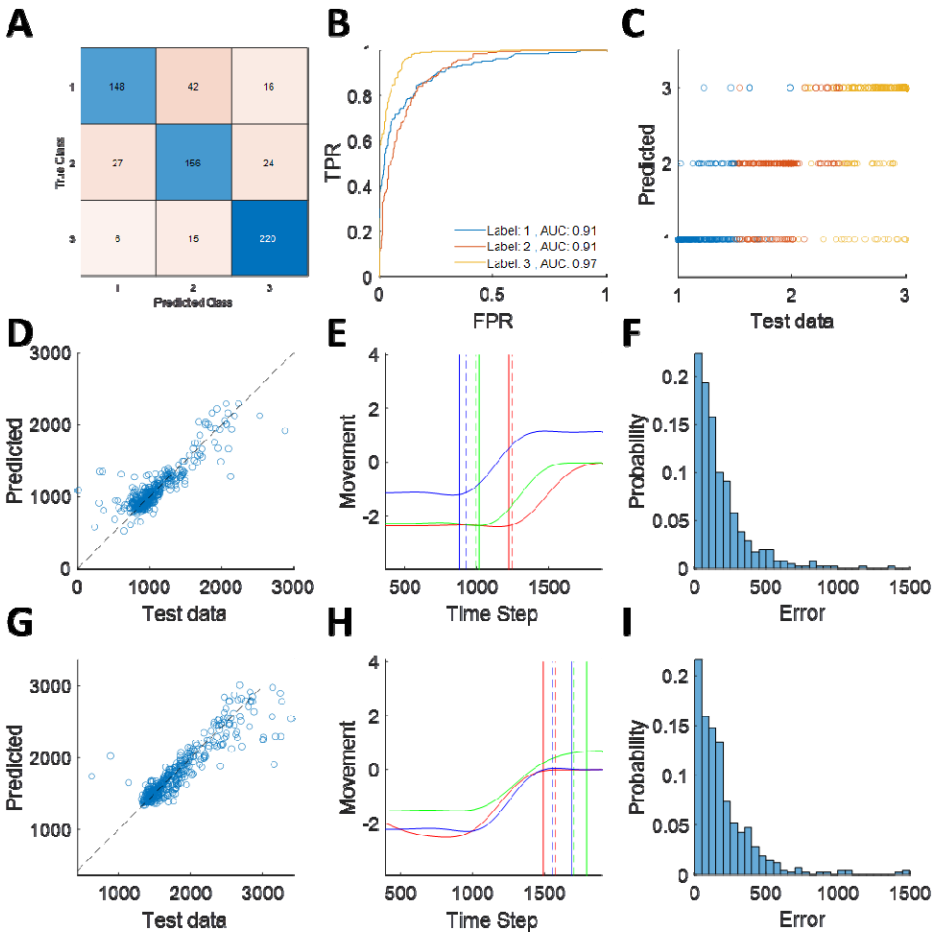

Supplementary Figure 1 – **Validation of convolutional neural network model for time locking of reaching movement.** Plots indicate results examining performance of a CNN based classifier/regression for reach quality (A-C); reach onset (exec.; D-F) and termination (hold; G-I). Training data was provided by manual labelling of data from three separate assessors on ~30% of the data. **(A)** Confusion matrix of recording quality class: (1) is optimal, (2) sub-optimal, (3) is rejected. See Appendix II for criteria. **(B)** Receiver operating characteristics for reach quality classifier, with each of the three data quality labels. **(C)** Scattergram of predicted vs test data. **(D)** Same as (C) but for prediction of reach onsets. **(E)** Example plot of three predicted (bold) vs manually marked (dashed) reach onsets. **(F)** Histogram of the model error (|predicted-manual|, ms). **(G-I)** Same as D-F, but for reach holds.

10.2 Supplementary Figure 2 – Analysis of Essential Tremor Properties

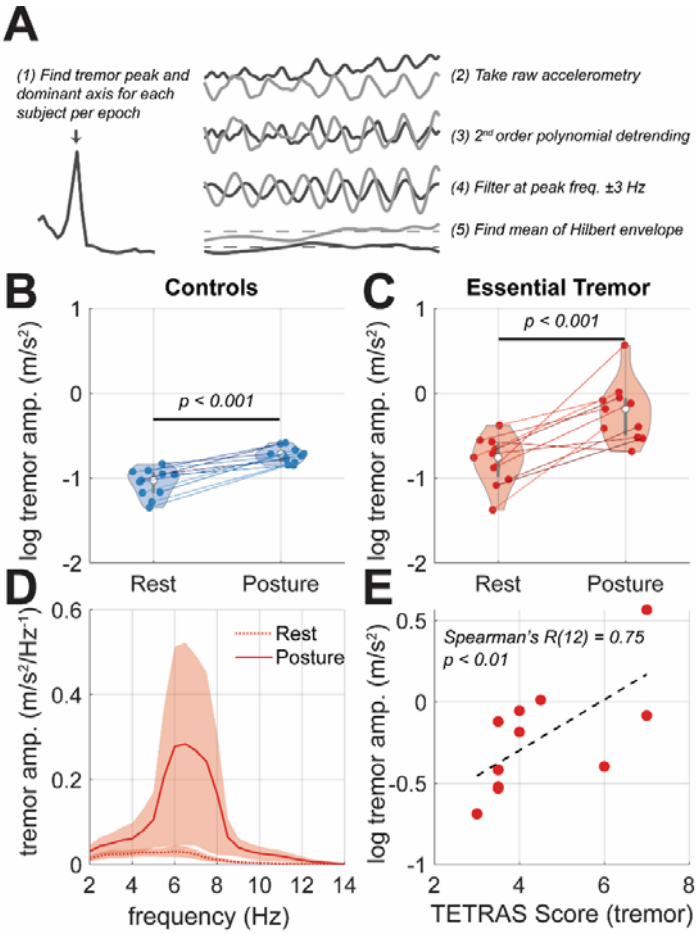

Supplementary Figure 2 – **Analysis of tremor dynamics during steady state recordings at rest and posture.** Violin plots indicate the distribution of tremor amplitudes over either the control (blue) or ET (red) cohorts), with lines linking individuals between rest and posture. Statistics indicate outcomes of paired t-tests. **(A)** Illustration of processing pipeline to compute the tremor amplitude. **(B)** Control subjects show a small increase in physiological tremor from rest to posture. **(C)** As expected from diagnosis, ET subjects show a significant increase in tremor at posture. **(D)** The average tremor peak frequency was around 6 Hz, increasing slightly during posture trials. Bounds give the SEM across ET patients. **(E)** Measures of tremor amplitude at posture positively correlate with clinical TETRAS assessment of tremor severity. A regression line is shown alongside, Spearman's correlation coefficient.

10.3 Supplementary Figure 3 –Effects of Experimental Conditions on Tremor

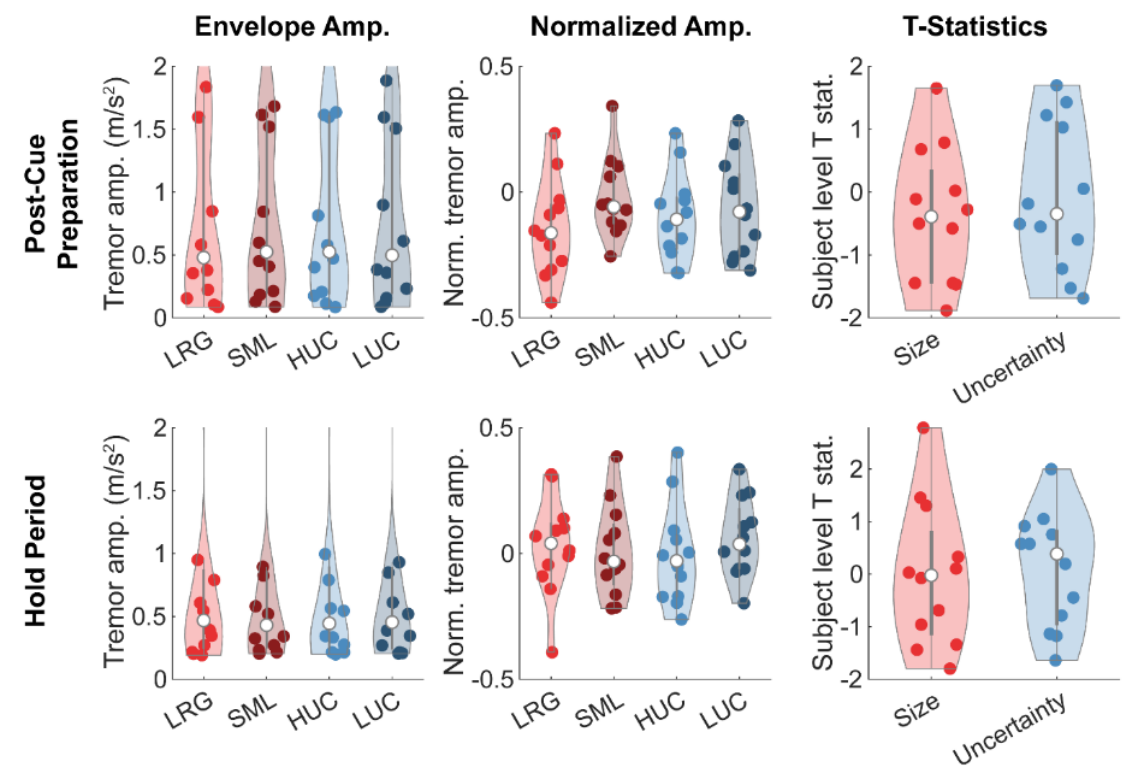

Supplementary Information 3 – **Analysis of modulation of tremor magnitude by task conditions.** Tremor magnitude was estimated as in Figure 2A. We divided trials by the 2x2 conditions modulating either target size (SML or LRG) and the uncertainty of directional cues (HUC or LUC). (1st Column) The violin plots here show the distribution of tremor power across the conditions. Each point represents the mean of an individual subject. (2nd Column) The distributions of tremor magnitude normalized by the subject level mean and standard deviation. (3rd Column) A plot of the subject level T-statistics comparing each of the experimental conditions. No significant differences between conditions were found.

10.4 Supplementary Figure 4 - Source level distribution of movement responsive beta power

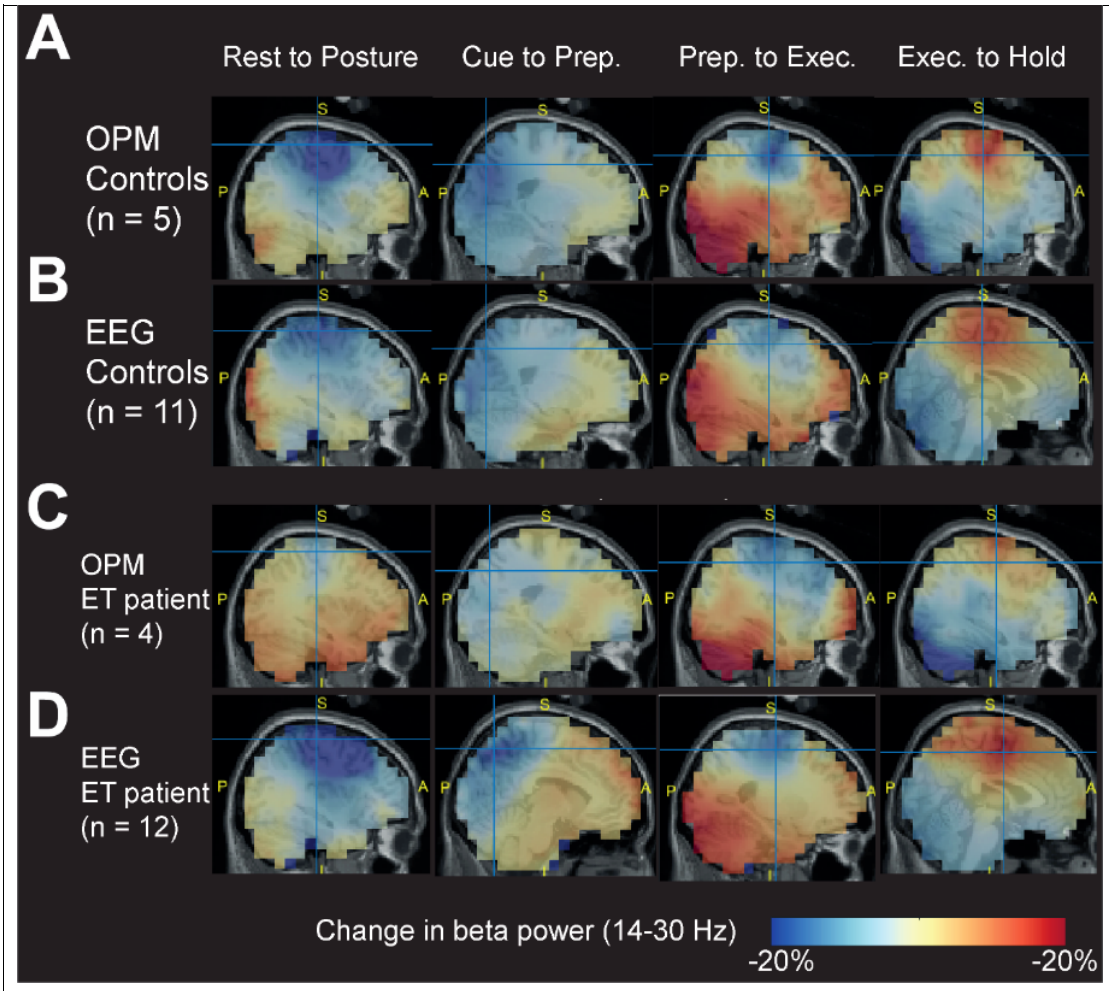

Supplementary Figure 4 – **Source level distribution of 14-30 Hz beta power.** Beta power was localized using a DICS beamformer. Differences in power relative to transitions during the reaching task were computed. Source images were normalized at a subject level before averaging. **(A)** Data for healthy controls recorded with OPMs; **(B)** healthy controls recorded with high density EEG; **(C)** Essential Tremor patients recorded with OPMs; **(C)** Essential Tremor patients recorded with high density EEG.

10.5 Supplementary Figure 5 - Spectrograms for Virtual Electrodes in Control Subjects

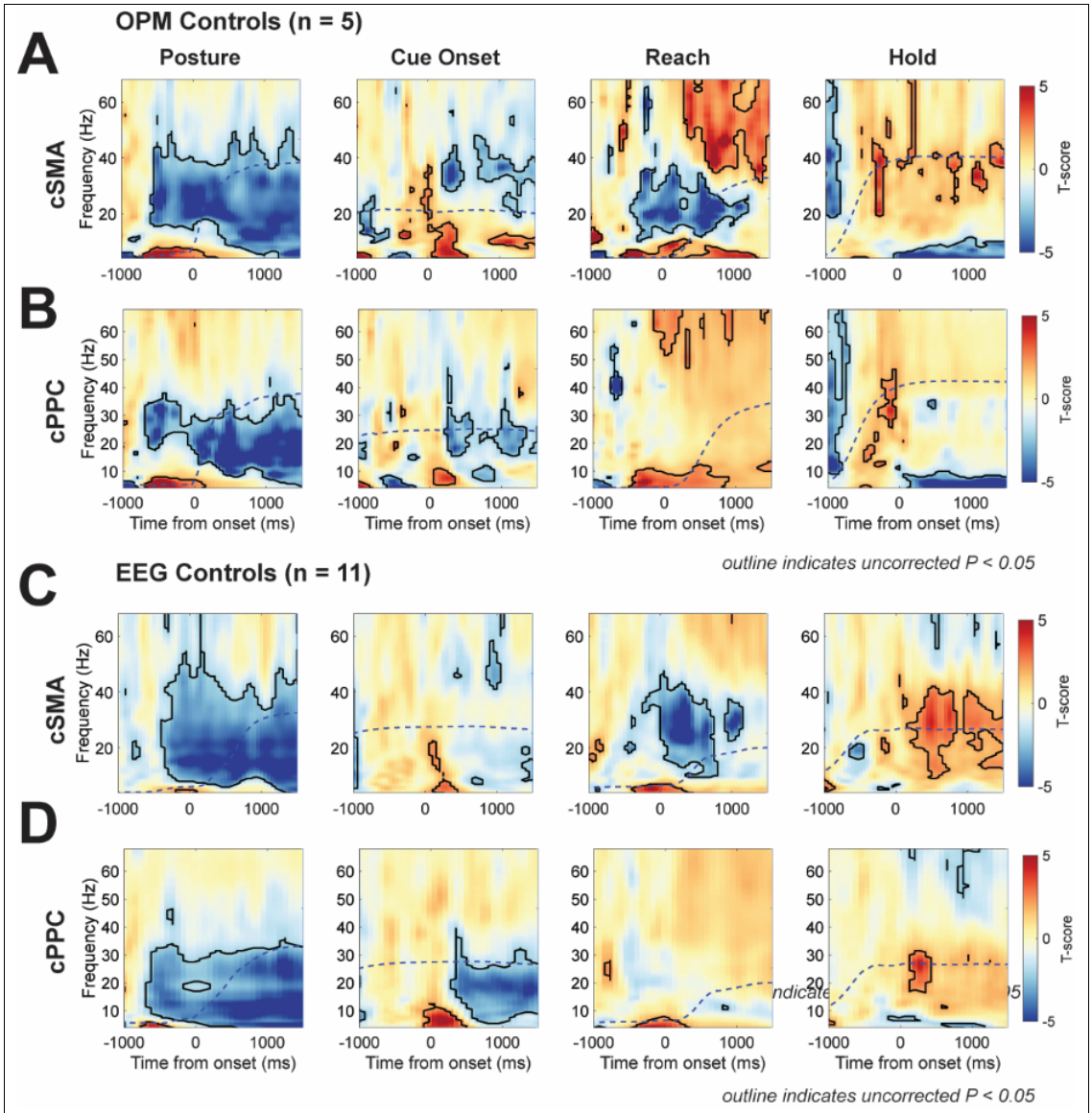

Supplementary Figure 5 - **Time-frequency spectrograms of time locked activity in either the cSMA or cPPC, in both OPM and EEG data in control subjects.** Panels show the group level t-statistics of time-frequency spectrograms constructed from virtual channels, compared to baseline. Bold outlines indicate thresholding on the critical T ($P < 0.05$; uncorrected). Dashed lines overlaid indicate the group averaged movement trace. **(A)** Spectrograms of OPM derived cSMA activity for time locked activity at onset of postural hold (1st column); onset of directional cues (2nd column); onset of reach (3rd column); and establishment of the hold period (4th column). **(B)** Same as (A), but for cPPC activity. **(C-D)** Same as A-B, but for EEG data.

10.6 Supplementary Figure 6 - Spectrograms for Virtual Electrodes in Essential Tremor Subjects

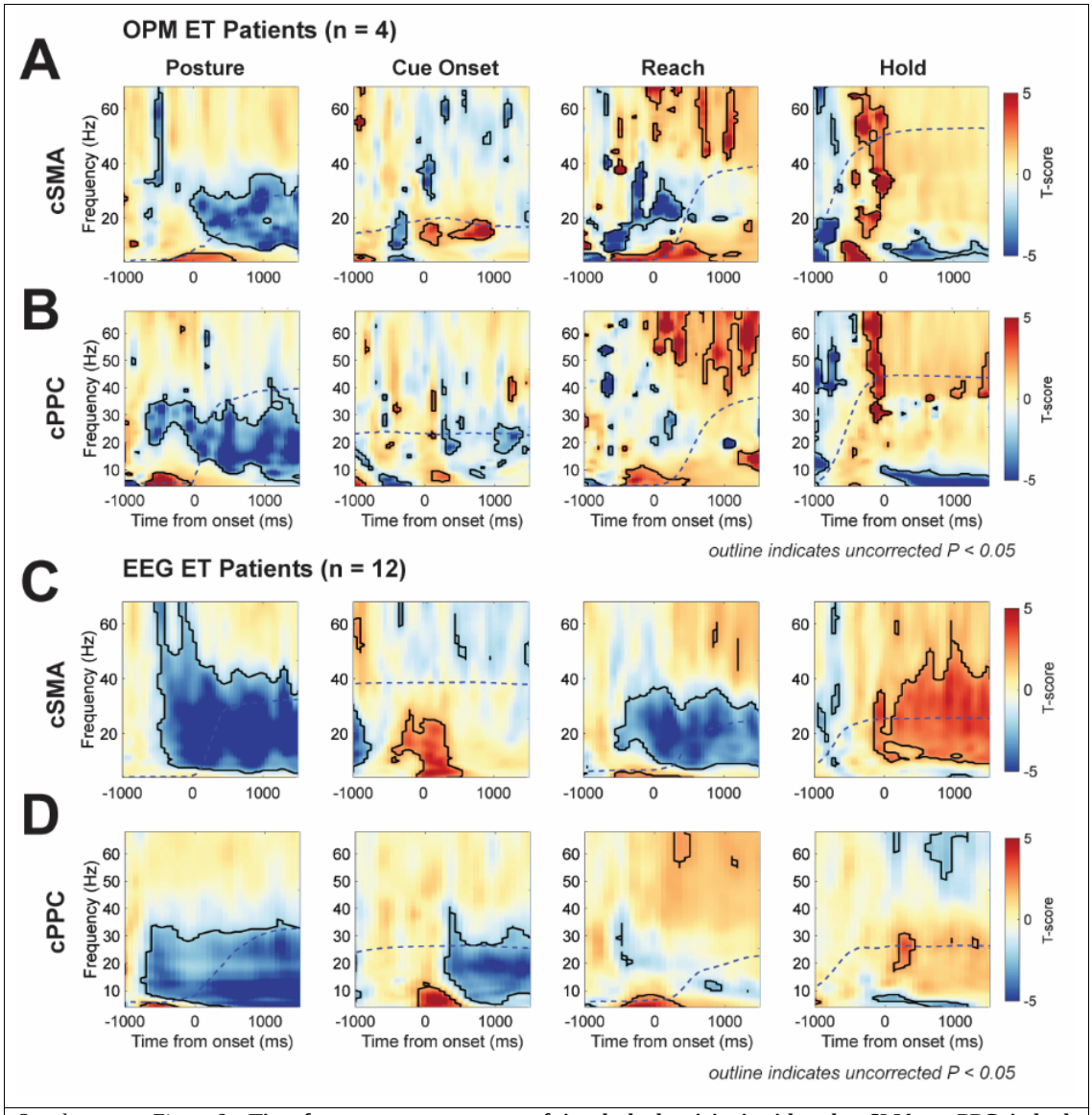

Supplementary Figure 6 – **Time-frequency spectrograms of time locked activity in either the cSMA or cPPC, in both OPM and EEG data in ET patients.** Panels show the group level t-statistics of time-frequency spectrograms constructed from virtual channels, compared to baseline. Bold outlines indicate thresholding on the critical T ($P < 0.05$; uncorrected). Dashed lines overlaid indicate the group averaged movement trace. **(A)** Spectrograms of OPM derived cSMA activity for time locked activity at onset of postural hold (1st column); onset of directional cues (2nd column); onset of reach (3rd column); and establishment of the hold period (4th column). **(B)** Same as (A), but for cPPC activity. **(C-D)** Same as A-B, but for EEG data.

10.7 Supplementary Figure 7– Alternative Comparisons of Movement Responsive Beta Activity

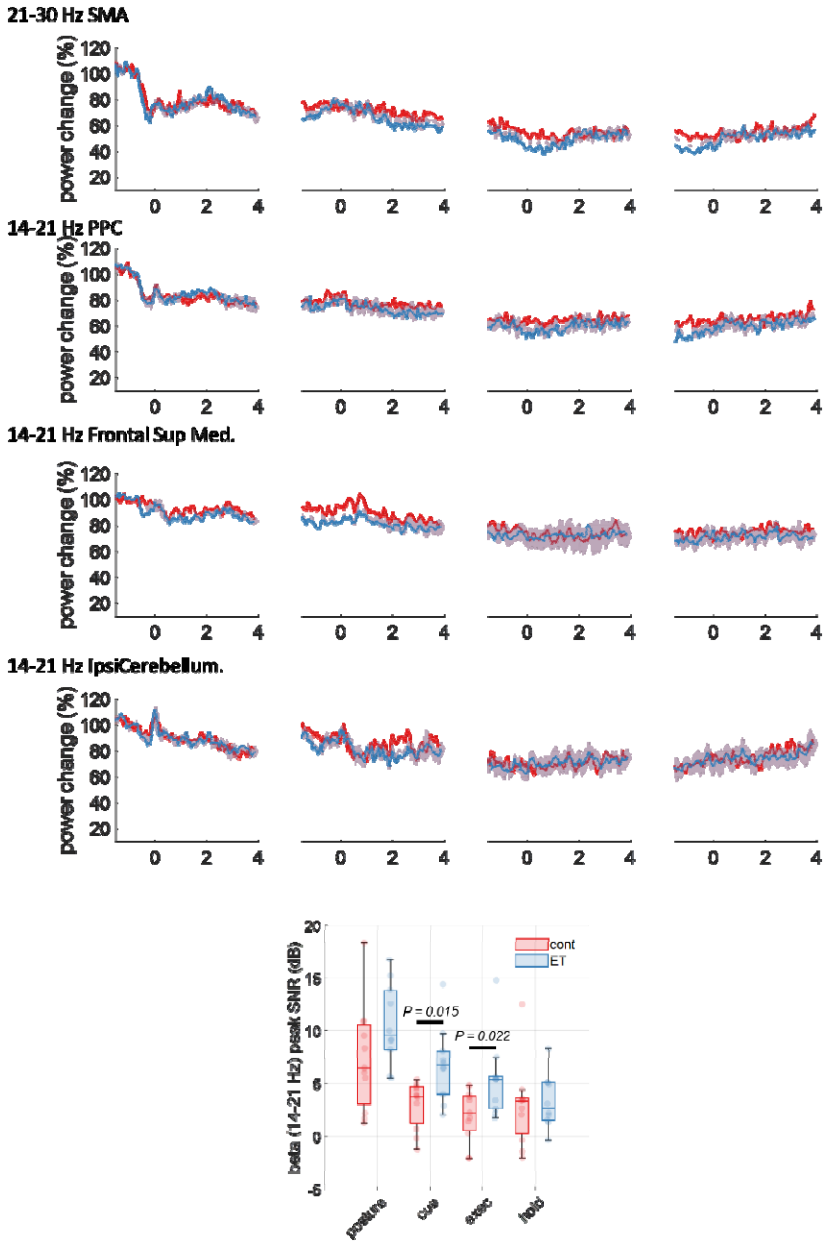

Supplementary Figure 7 – **Movement related beta desynchronization** in (A) Upper beta (21-30 Hz) band in the contralateral SMA; and lower beta band (14-21 Hz) in the: (B) contralateral posterior parietal cortex, (C) frontal superior medial cortex, (D) and ipsilateral cerebellum VI. (E) Comparison of absolute power in terms of the ratio of peak (14-21 Hz) to tail (30-48 Hz) SNR.

10.8 Supplementary Figure 8 – Comparison of Movement Related Beta Dynamics in Patients vs Controls in OPM Data

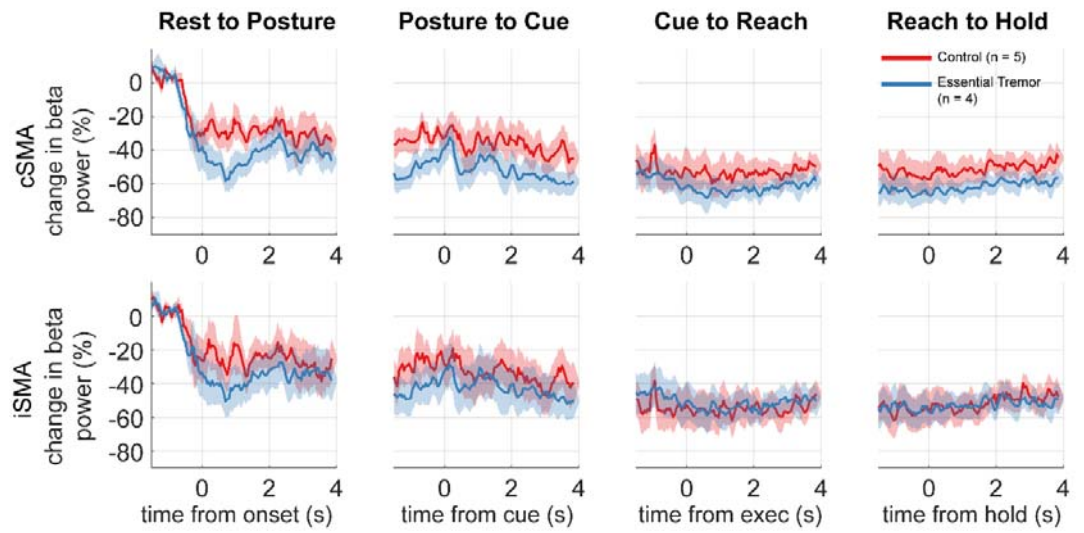

Supplementary Figure 8 – **Analysis comparing movement-induced beta desynchronization in the contralateral supplementary motor area (cSMA) between Essential Tremor (ET) patients and Control recordings in OPM. (A)** Time courses of low beta power (14-21 Hz) in the cSMA, scales as the percentage change relative to at rest (0%), shown across the postural hold, reach planning, execution, and the hold period ($1^{st,}$ 2nd, $3^{rd,}$ and 4th columns, respectively). Data is shown as the group average ±SEM, for either control (red) or ET patients (blue). Bars indicate significant differences between controls and ETs, determined by cluster permutation statistics ($P < 0.05$). **(B)** Same as (A), but for ipsilateral SMA.

10.9 Supplementary Figure 9 – Comparison Of Whole Brain, Motor Responsive Latent Networks Between Controls and ET Patients Using OPM Data

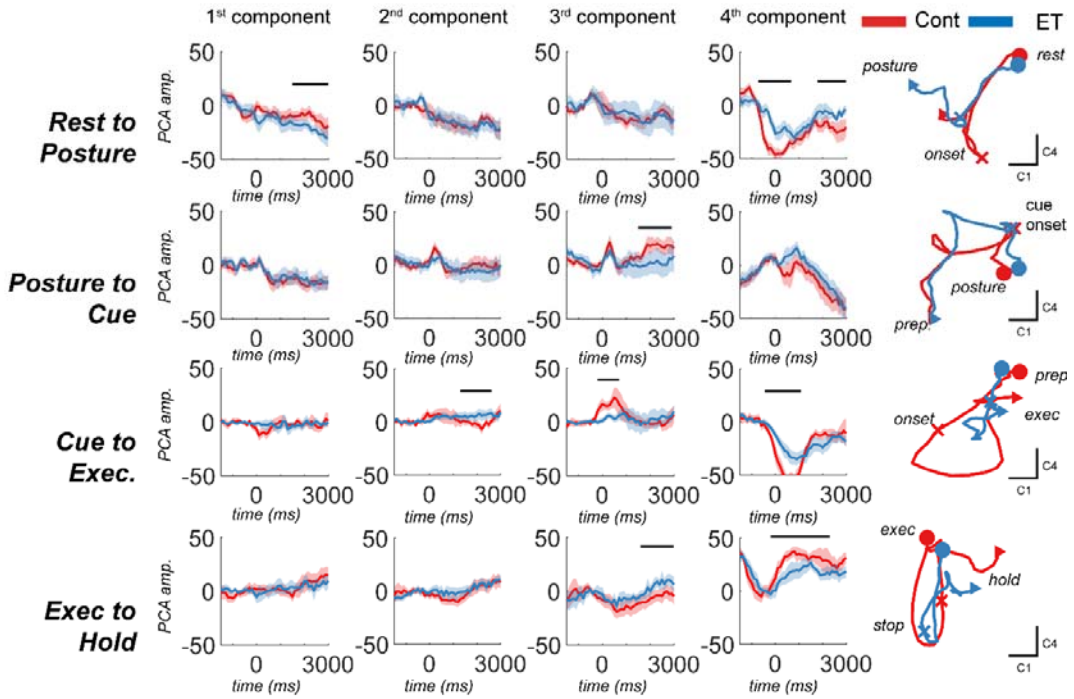

Supplementary Figure 9 –**Visualization of whole brain, motor responsive, latent dynamics and a comparison between controls and patients with ET recorded with OPM.** Components were computed using tfPCA applied to the group averaged EEG data (Figure 5). These coefficients were then used to project data to trial-level latent dynamics that could be used to explore differences between controls and ET patients. **(A)** The latent dynamics exhibited during the postural hold for each component (columns) are plot for ET (blue) and controls (red) separately. Bars and associated P-values indicate the outcome of cluster permutation statistics between the two experimental groups. **(B-D)** Same as (A) but for cue presentation, reach execution, and the sustained hold. **(E-H)** Plots of the 2D latent trajectories (components 1 and 4, only) indicate highly correlated dynamics between controls and ETs with quantitative differences in the weighting of the components such as increased engagement of the prefrontal beta network in ET subjects (4th component, apparent in plot G).

11 Appendices

11.1 Appendix I – Clinical Table: EEG Patients

Subject	Age	Gender	TETRAS Performance	TETRAS Upper Limb Tremor (R/L)	TETRAS Head Tremor	Medication
1	53	M	12.5	3.5/3	0	Gabapentin 600 mg; Primidone 500mg; Amitriptyline
2	73	M	15.5	3/4	1	Primidone 150mg; Propranolol 40mg; L-Thyrpx 100mg; Ramipril 2.5 mg
3	68	M	23	4/6	0	Propranolol 40mg
4	59	M	38	6.5/8	1	Propranolol 80mg; Amlodipine 5mg; Insulin Glargine + Lispro; Clopidogrel 75mg; Simva 20mg; Ramipril 10mg
5	19	F	7.5	1/3.5	0	None
6	19	M	11	3/3	0	None
7	58	F	15.5	3/4	1	Propranolol 10mg; Escitalopram 15mg
8	24	F	9	3.5/3	0	None
9	21	F	17	3.5/7	0	Propranolol 10mg
10	61	M	27.5	7/6	2	Propranolol 40mg; Liskantin 250mg
11	42	M	14	4.5/4.5	0	None
12	64	F	13	3/3.5	1	Propranolol 20mg

11.2 Appendix II – Clinical Table: OPM Patients

Subject	Age	Gender	TETRAS Performance	TETRAS Upper Limb Tremor	TETRAS Head	Medication

				(R/L)	Tremor	
1	67	F	19	5/4	0	None
2	44	F	25	7/7	0	None
3	66	M	17	6/6	0	Amlopidine, Pravastatin, NiC for tremor
4	25	F	17	3/6		Primidone 25 mg

11.3 Appendix III – Algorithm to Manipulate Cue Uncertainty

Let D be the set of cardinal directions, where $D = \{N, NE, E, SE, S, SW, W, NW\}$. A direction d is selected from D, where $d \in D$. We generate a set of N random phases (expressed in radians):

$$\theta_n = \bar{\theta} + \sigma\epsilon_n, \qquad n = 1,2, \dots, N$$

where $\bar{\theta}$ and σ represent the chosen angle and dispersion (uncertainty) of the movement cues, and ϵ_n is a random variable sampled from a standard normal distribution, $\epsilon_n \sim N(0,1)$. The direction of each arrow is then wrapped around the unit circle: $\phi_n = \arg\left(e^{i\theta_n}\right)$. Finally the arrow directions are then taken by computing the normalized histogram for bins with edges corresponding to the cardinal directions, to yield a scalar for each arrow. We used $\sigma = 0.98$ for low uncertainty trials, and $\sigma = 1.64$ for high uncertainty trials, yielding 85% and 15% average success rates in piloting with healthy controls.

11.4 Appendix IV – Criteria for Reach Quality Marking

Grade 1 – Optimal Reach

- A stable baseline is present prior to movement, with little oscillation or prepotent movement.
- The reach may be initiated before the movement cue (i.e., t < 0) if baseline is stable.
- The reach itself is smooth, with a clear stereotyped trajectory.
- The hold period is stable and lasts greater than 2 seconds, with no clear drifts or repositioning of the hand.

Grade 2 – Suboptimal Reach

- A baseline period is apparent, although some slow drifts in posture, or small prepotent movements are present.
- The reach may be initiated before the movement cue (i.e., t < 0) if the baseline is stable.
- The reach is jerky, or non-smooth containing mid-reach corrections and changes in velocity.
- The hold period is apparent and last for a duration >= 2 seconds. The hold period may contain slow drifts, or small corrective movements.

Grade 3 – Rejected Reach

- The reach is extremely slow (> 4 seconds).
- The reach is extremely jerky/non-smooth.
- There is no clear baseline periods lasting > 2 seconds.

- There is no clear hold period lasting > 2 seconds.

11.5 Appendix V – Details of Source Estimation Techniques

Source inversion of sensor-level data involves constructing forward models to simulate the propagation of neural activity from the source to the sensor. For EEG data, we used a template boundary element model with sensor locations set according to the 10-10 system. For OPM data, sensor positions were derived from custom head cast models aligned to the subject's structural MRIs. For the two subjects lacking MRIs, sensors were transformed to a template space using an iterative closest point algorithm to match the 3D scanned scalp to the template model. OPM head models used the single shell method[103]. To facilitate group-level statistical comparisons, a nonlinear warping was applied to align the anatomical scans.

Subject level common filters were computed from data concatenated across the multiple epochs of the experiment. Covariance matrices were computed in two frequency bands: tremor (peak postural tremor frequency ±1.5 Hz) and wide band beta (14-30 Hz). Each covariance matrix was truncated by its effective rank[104]. A covariance regularization of 1% was used.

11.6 Appendix VI – Implementation of Time Frequency Principle Component Analysis

tfPCA was applied to the group-averaged data with spectrograms concatenated for each motor epoch (time x four epochs). To avoid low frequency bias due to 1/f structure of EEG/OPM, spectra were log scaled. Spectrograms were also Z-normalized per subject to remove differences in SNR. We then constructed an $n \times p$ matrix $\boldsymbol{X}$ ([n: concatenated time] x [p: channel x frequency]) to which we applied PCA to yield coefficients $\boldsymbol{V}$ (p x number of components) for each spatio-spectral component, and latent scores $\boldsymbol{Z}$ (component x time). PCA coefficients were rotated using the Varimax algorithm to aid interpretability. We then projected components from the single trial level data D_t (to compare experimental conditions and perform regressions) by computing $Z_t = \boldsymbol{V}D_t$. We also reconstructed components in the time frequency domain by multiplying trial-level data with the projection matrix $\boldsymbol{P} = \boldsymbol{V}\boldsymbol{V}^{\boldsymbol{T}}$, which we used for CNN tremor prediction analyses. In this way, the coefficients derived from the group averaged EEG data were used to project both EEG and OPM data to single trial level components.

11.7 Appendix VII- CNN Decoding Performance- with EEG Data

Table 1 - Between-Subject CNN Decoding of Tremor Severity using EEG Virtual Channels

Between-Subject CNN Decoding of Tremor Severity using EEG Virtual Channels- (R^2, mean averaged over 5 runs)							
Virtual Channel	**Posture**	**Grad-CAM Feat**	**Cue**	**Grad-CAM Feat**	**Hold**	**Grad-CAM Feat**	Average
cSMA	0.174	low beta	0.156	tremor	0.088	tremor/high beta	*0.139*
cPPC	0.250	low beta	0.170	tremor/high beta	0.024	tremor	*0.148*
dlPFC	0.092	low beta	0.156	low beta	0.067	gamma	*0.105*
iCer V6	0.132	tremor	0.039	tremor	0.061	tremor	*0.077*
Average	*0.162*		*0.130*		*0.060*		***0.117***

Table 2 - Within-Subject CNN Decoding of Tremor Severity using EEG Virtual Channels

Within-Subject CNN Decoding of Tremor Severity using EEG Virtual Channels- (R^2, mean averaged over 5 runs)-							
Virtual Channel	**Posture**	**Grad-CAM Feat**	**Cue**	**Grad-CAM Feat**	**Hold**	**Grad-CAM Feat**	**Average**
cSMA	0.006		0.002		0.009		*0.006*
cPPC	0.002		0.009		0.025		*0.012*
dlPFC	0.002		0.002		0.009		*0.004*
iCer V6	0.003		0.006		0.017		*0.009*
Average	*0.003*		*0.005*		*0.015*		***0.008***

Table 3 - Between-Subject CNN Decoding of Tremor Severity using Principal Components

Between-Subject CNN Decoding of Tremor Severity Using EEG Principal Components- (R^2, mean averaged over 5 runs)							
Comp.	**Posture**		**Cue**		**Hold**		Average
Comp. 1	0.254		0.028		0.078		*0.120*
Comp. 2	0.061		0.114		0.048		*0.075*
Comp. 3	0.157		0.100		0.011		*0.088*
Comp. 4	0.067		0.042		0.111		*0.073*
Average	*0.135*		*0.070*		*0.062*		***0.089***

Table 4 - Within-Subject CNN Decoding of Tremor Severity using EEG Principal Components

Within-Subject CNN Decoding of Tremor Severity Using EEG Principal Components- (R^2, mean averaged over 5 runs)							
Comp.	**Posture**		**Cue**		**Hold**		Average
Comp. 1	0.003		0.004		0.027		*0.011*
Comp. 2	0.003		0.010		0.029		*0.014*
Comp. 3	0.002		0.006		0.027		*0.012*
Comp. 4	0.003		0.007		0.032		*0.014*
Average	*0.003*		*0.007*		*0.029*		***0.013***

11.8 Appendix VIII- CNN Decoding Performance- with OPM Data

Table 1 - Between-Subject CNN Decoding of Tremor Severity using OPM Virtual Channels

Between-Subject CNN Decoding of Tremor Severity using OPM Virtual Channels- (R, mean averaged over 5 runs)							
Virtual Channel	**Posture**	**Grad-CAM Feat**	**Cue**	**Grad-CAM Feat**	**Hold**	**Grad-CAM Feat**	*Average*
cSMA	-0.064		-0.058		0.062		*-0.020*
cPPC	0.096		0.194		0.638		*0.309*
dlPFC	0.267		0.116		0.085		*0.156*
iCer V6	0.412		0.104		0.347		*0.288*
Average	*0.178*		*0.089*		*0.283*		***0.183***

Table 2 - Within-Subject CNN Decoding of Tremor Severity using OPM Virtual Channels

Within-Subject CNN Decoding of Tremor Severity using OPM Virtual Channels- (R^2, mean averaged over 5 runs)-							
Virtual Channel	**Posture**	**Grad-CAM Feat**	**Cue**	**Grad-CAM Feat**	**Hold**	**Grad-CAM Feat**	*Average*
cSMA	0.005		0.010		0.022		*0.012*
cPPC	0.013		0.012		0.010		*0.011*
dlPFC	0.004		0.003		0.053		*0.020*
iCer V6	0.008		0.010		0.115		*0.044*
Average	*0.008*		*0.009*		*0.050*		***0.022***

Table 3 - Between-Subject CNN Decoding of Tremor Severity using OPM Principal Components

Between-Subject CNN Decoding of Tremor Severity Using OPM Principal Components- (R^2, mean averaged over 5 runs)							
Comp.	**Posture**		**Cue**		**Hold**		Average
Comp. 1	0.043		0.003		0.012		*0.020*
Comp. 2	0.020		0.057		0.048		*0.042*
Comp. 3	0.052		0.037		0.052		*0.047*
Comp. 4	0.027		0.001		0.115		*0.048*
Average	*0.036*		*0.024*		*0.057*		***0.039***

Table 4 - Within-Subject CNN Decoding of Tremor Severity using OPM Principal Components

Within-Subject CNN Decoding of Tremor Severity Using OPM Principal Components- (R^2, mean averaged over 5 runs)							
Comp.	**Posture**		**Cue**		**Hold**		Average
Comp. 1	0.008		0.008		0.004		*0.006*
Comp. 2	0.010		0.009		0.035		*0.018*
Comp. 3	0.003		0.009		0.026		*0.013*
Comp. 4	0.001		0.016		0.007		*0.008*
Average	*0.006*		*0.010*		*0.018*		***0.011***

11.9 Appendix IX – Analysis of Reproducibility of Latent Dynamics

Table 1 – Analysis of Correlation Between Latent Dynamics in Controls and ET Recordings

	EEG				
	Comp 1	**Comp 2**	**Comp 3**	**Comp 4**	*Average*
Posture	0.96	0.98	0.98	0.94	*0.96*
Cue	0.91	0.95	0.68	0.86	*0.85*
Reach	0.90	0.98	0.91	0.95	*0.94*
Hold	0.88	0.90	0.88	0.98	*0.91*
Average	*0.91*	*0.95*	*0.86*	*0.93*	***0.91***

	OPM				
	Comp 1	**Comp 2**	**Comp 3**	**Comp 4**	*Average*
Posture	0.90	0.90	0.83	0.88	*0.88*
Cue	0.96	0.68	0.42	0.97	*0.76*
Reach	0.84	0.85	0.89	0.94	*0.88*
Hold	0.87	0.90	0.76	0.85	*0.85*
Average	*0.89*	*0.83*	*0.73*	*0.91*	***0.84***

Table 2 – Analysis of Correlation Between Latent Dynamics in OPM and EEG

Analysis of Correlation Between Latent Dynamics in OPM and EEG (Pearson's Correlation Coefficient R)					
	Component 1	**Component 2**	**Component 3**	**Component 4**	*Average*
Posture	0.93	0.72	0.65	0.93	*0.81*
Cue	0.94	0.62	0.47	0.99	*0.76*
Reach	0.97	-0.03	0.46	0.94	*0.59*
Hold	0.93	0.56	0.65	0.87	*0.75*
Average	*0.94*	*0.47*	*0.56*	*0.93*	***0.73***

11.10 Appendix X– Comparison of Source Localized Power in OPM and EEG Data

Source localization of task related power changes was compared between EEG and OPM data. We examined the consistency of source estimates in terms of the intertrial correlation coefficients per subject. This was estimated by taking the average of the pairwise Pearson correlations between volumetric estimates obtained with the beamformer for each trial. We also examined the spatial properties of the beamformer images using the sharpness ratio. Briefly, 3D Fourier transforms of each trial level source image was computed. The ratio of power at high and low frequencies then indexes the "sharpness" of the image. We set the threshold between high and low frequency at 40% of the maximum frequency. We also examined effect sizes obtained, comparing the average and range of t-statistics measured when contrasting with a baseline (see main text). Significant differences between OPM and EEG images were compared using t-statistics. The results are shown below.

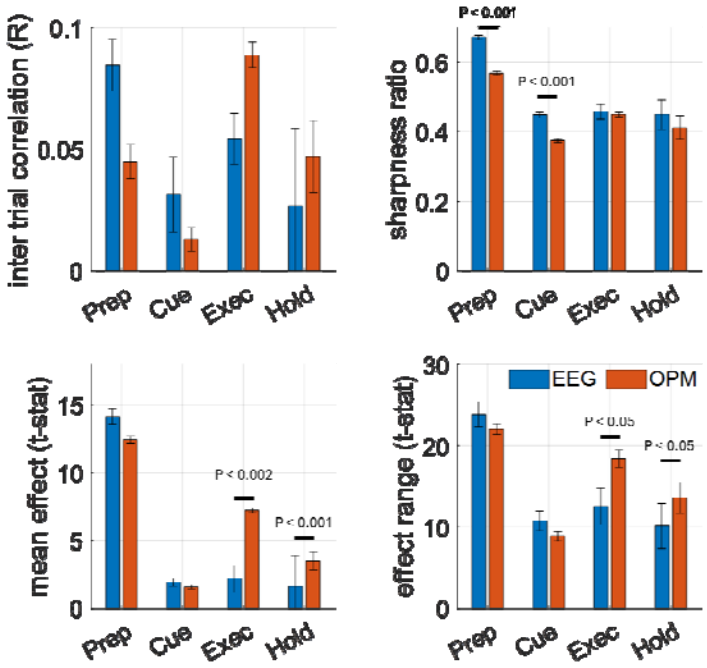

No significant differences were found between OPM and EEG for intertrial correlations. EEG images were significantly sharper, but only for epochs involving movement preparation, and cue onsets. OPM effect sizes were however bigger, particularly at periods involving large reaching movements during execution and hold.

11.11 Appendix XI– Details of 3rd Party Toolboxes

Toolbox Name	Author	Year	Source/Reference
boundedline-pkg	Kelly Kearney	2015	https://github.com/kakearney/boundedline-pkg
brewermap	Stephen Cobeldick	2014	https://github.com/DrosteEffect/BrewerMap
Fieldtrip	Donders Institute, Radbound University	2020	https://www.fieldtriptoolbox.org/
linspecer	Jonathan C. Lansey	2015	https://github.com/davidkun/linspecer
Matlab Toolbox for Dimensionality Reduction (v0.8.1b)	Laurens van der Maaten	2013	https://lvdmaaten.github.io/drtoolbox/

splitvec	Bruno Luong	2009	https://uk.mathworks.com/matlabcentral/fileexchange/24255-splitvec
SPM 12	Wellcome Centre for Human Neuroimaging, University College London	2020	https://www.fil.ion.ucl.ac.uk/spm/